Article

Fluorescence and Aggregation Behavior of Poly(amidoamine) Dendrimers Peripherally Modified with Aromatic Chromophores: the Effect of Dendritic Architectures

Bing-Bing Wang, Xin Zhang, Xin-Ru Jia, Zi-Chen Li, Yan Ji, Ling Yang, and Yen Wei

J. Am. Chem. Soc., **2004**, 126 (46), 15180-15194• DOI: 10.1021/ja048219r • Publication Date (Web): 29 October 2004

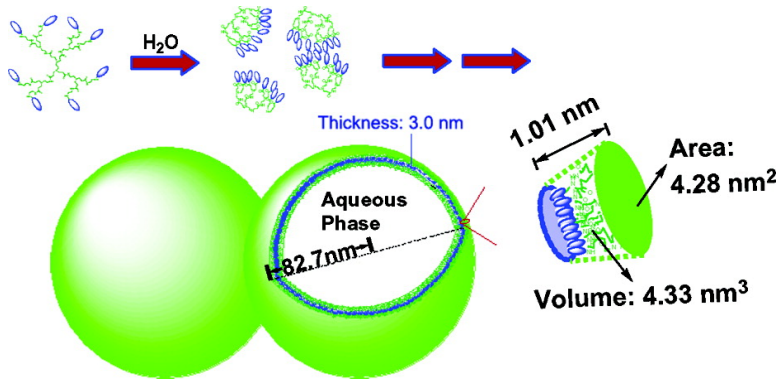

More About This Article

Additional resources and features associated with this article are available within the HTML version:

- Supporting Information
- Links to the 6 articles that cite this article, as of the time of this article download
- Access to high resolution figures
- Links to articles and content related to this article
- Copyright permission to reproduce figures and/or text from this article

View the Full Text HTML

J|A|C|S
ARTICLES
Published on Web 10/29/2004

Fluorescence and Aggregation Behavior of Poly(amidoamine) Dendrimers Peripherally Modified with Aromatic Chromophores: the Effect of Dendritic Architectures

Bing-Bing Wang,[†] Xin Zhang,[†] Xin-Ru Jia,*[,†] Zi-Chen Li,[†] Yan Ji,[†] Ling Yang,[†] and Yen Wei*[,‡]

Contribution from the Department of Polymer Science and Engineering, College of Chemistry and Molecular Engineering, Peking University, Beijing 100871, China, and Department of Chemistry, Drexel University, Philadelphia, Pennsylvania 19104

Received March 29, 2004; E-mail: xrjia@chem.pku.edu.cn; weiyen@drexel.edu

Abstract: PAMAM dendrimers of the zeroth to fifth generation (G0−5) have been peripherally modified with phenyl, naphthyl, pyrenyl, and dansyl chromophores. Their fluorescence behaviors are strongly affected by the dendritic architectures at different generations. These dendrimers modified with hydrophobic chromphores can self-organize into vesicular aggregates at the low generations G0−3 in water. The size and aggregation number of these vesicles decrease with increasing generation from G0 to G3. Critical aggregation concentration determined by fluorescence spectroscopy reveals that these aggregates can be favorably formed in the order of G3 > G2 > G1. In contrast to the vesicles made from traditional amphiphilic compounds, these dendrimer-based vesicles are very adhesive due to the H-bonding interaction and entanglement of dendritic branches located in the outer layer. A large number of multivesicle assemblies, i.e., "twins" and "quins" consisting of two and five vesicles, were clearly identifiable with transmission electron (TEM) and atomic force microscopy. For the dendrimers with peripheral pyrenyl chromophores, triangle-like vesicles were observed in water. The hydrophobic interphase thickness of the vesicular bilayer is ca. 2.0−3.2 nm determined by fluorescence resonance energy transfer methods, which agrees well with the thickness directly observed with TEM.

Introduction

Since the pioneering work by Tomalia[1] and Vögtle[2] about 20 years ago, we have witnessed an explosive growth of a new class of highly symmetric and branched, monodisperse, aesthetically appealing macromolecules with well-defined shape and size, i.e., dendrimers.[3] Recent research emphasis seems to shift from the synthesis of novel dendrimers to their properties and potential applications.[4] Modification and functionalization of dendritic periphery are of particular keys to tune and manipulate the properties of dendrimers such as solubility and viscosity as well as photochemical and photophysical behavior.[5] The average spacing between peripheral chromophores can be controlled by varying the dendrimer generations.

A large number of papers have reported on the peripheral modification of dendrimers with various moieties such as azobenzene,[6] dansyl sulfonate,[7] glucose,[8] porphyrins,[9] cyanobiphenyl mesogens,[10] oligo(*p*-phenylene vinylene),[11] aromatic amines,[12] and cumarin.[13] The peripheral modification of dendrimers with photo- and/or electroactive moieties generally resulted in interesting specific functions. Compared to their linear analogues, the unusual molecular architecture of dendritic polymers provides a suitable framework to achieve unique photochemical and photophysical properties. As examples,

[†] Peking University.
[‡] Drexel University.

(1) Tomalia, D. A.; Baker, H.; Dewald, J. R.; Hall, M.; Kallos, G.; Martin, S.; Roeck, J.; Ryder, J.; Smith, P. *Polym. J.* **1985**, *17*, 117−132.
(2) Buhleier, E. W.; Wehner, W.; Vögtle, F. *Synthesis* **1978**, 155−158.
(3) (a) Newkome, G. R.; Moorefield, C. N.; Vögtle, F. *Dendritic Molecules*: *Concepts, Syntheses and Perspectives*; VCH: Weinheim, Germany, 1996. (b) Fréchet, J. M. J.; Tomalia, D. A. *Dendrimers and Other Dendritic Polymers*; John Wiley & Sons Ltd.: 2002.
(4) For selected reviews: (a) Sugiura, K. *Top. Curr. Chem.* **2003**, *228*, 65−85. (b) Balzani, V.; Ceroni, P.; Maestri, M.; Saudan, C.; Vicinelli, V. *Top. Curr. Chem.* **2003**, *228*, 159−191. (c) Crooks, R. M.; Zhao, M. Q.; Sun, L.; Chechik, V.; Yeung, L. K. *Acc. Chem. Res.* **2001**, *34*, 181−190.
(5) Grayson, S. K.; Frechet, J. M. J. *Chem. Rev.* **2001**, *101*, 3819−3867.
(6) Tsuda, K.; Dol, G. C.; Gensch, T.; Hofkens, J.; Latterini, L.; Weener, J. W.; Meijer, E. W.; de Schryver, F. C. *J. Am. Chem. Soc.* **2000**, *122*, 3445−3452.
(7) (a) Vicinelli, V.; Ceroni, P.; Maestri, M.; Balzani, V.; Gorka, M.; Vogtle, F. *J. Am. Chem. Soc.* **2002**, *124*, 6461−6468. (b) Teobaldi, G.; Zerbetto, F. *J. Am. Chem. Soc.* **2003**, *125*, 7388−7393. (c) Balzani, V.; Ceroni, P.; Gestermann, S.; Kauffmann, C.; Gorka, M.; Vogtle, F. *Chem. Commun.* **2000**, *122*, 853−854.
(8) Schmitzer, A.; Perez, E.; Rico-Lattes, I.; Lattes, A.; Rosca, S. *Langmuir* **1999**, *15*, 4397−4403.
(9) Yeow, E. K. L.; Ghiggino, K. P.; Reek, J. N. H.; Crossley, M. J.; Bosman, A. W.; Schenning, A. P. H. J.; Meijer, E. W. *J. Phys. Chem. B* **2000**, *104*, 2596−2606.
(10) (a) Ponomarenko, S. A.; Boiko, N. I.; Shibaev, V. P.; Richardson, R. M.; Whitehouse, I. J.; Rebrov, E. A.; Muzafarov, A. M. *Macromolecules* **2000**, *33*, 5549−5558. (b) Baars, M. W. P. L.; Sontjens, S. H. M.; Fischer, H. M.; Peerlings, H. W. I.; Meijer, E. W. *Chem.—Eur. J.* **1998**, *4*, 2456−2466.
(11) Schenning, A. P. H. J.; Peeters, E.; Meijer, E. W. *J. Am. Chem. Soc.* **2000**, *122*, 4489−4495.
(12) Freeman, A. W.; Koene, S. C.; Malenfant, P. R. L.; Thompson, M. E.; Frechet, J. M. J. *J. Am. Chem. Soc.* **2000**, *122*, 12385−12386.
(13) (a) Adronov, A.; Gilat, S. L.; Frechet, J. M. J.; Ohta, K.; Neuwahl, F. V. R.; Fleming, G. R. *J. Am. Chem. Soc.* **2000**, *122*, 1175−1185. (b) Gilat, S. L.; Adronov, A.; Frechet, J. M. J. *Angew. Chem., Int. Ed.* **1999**, *38*, 1422−1427.

 10.1021/ja048219r CCC: $27.50

Scheme 1. Peripheral Modification of PAMAM Dendrimers with Phenyl, Naphthyl, Pyrenyl, and Dansyl Chromophores[a]

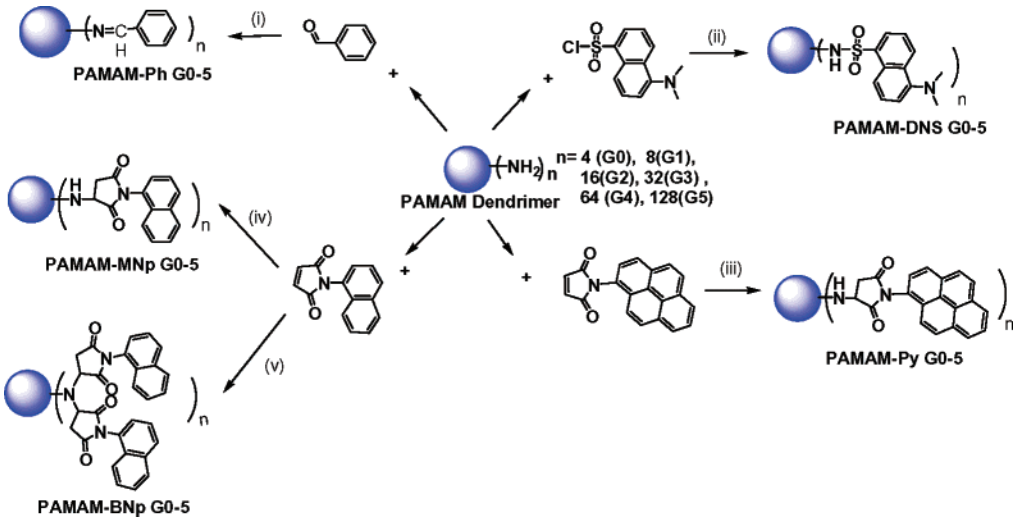

[a] Reagents and conditions: (i) methanol, Na_2SO_4, 60 °C; (ii) methanol, 30 °C, NaOH; (iii−v) acetone/methanol (4:1 v/v), room temperature, 24 h.

Crooks and Baker[14] prepared the poly(propylene imine) dendrimers functionalized with pyrene chromophores and studied the correlation of spectroscopic properties with dendrimer structures. Moore and co-workers[15a−c] studied the energy migration in phenylacetylene dendrimers having perylene chromophores. Fox and co-workers[15d] modified fan-shaped polyether dendrons with pyrene and naphthalene chromophores and studied the fluorescence resonance energy transfer between the core and peripheral chromophores. Frechet and co-workers[5,16] synthesized a series of dendrimers bearing light-harvesting chromophores at their periphery, which can transfer outer energy to a central core. Beyond any doubt, a better understanding of the photochemical and photophysical behaviors of the peripherally modified dendrimers and their structure−property relationship is necessary and of great significance in order to develop innovative applications for these unique molecules.

On the other hand, amphiphilic dendrimers have recently attracted an enormous amount of attention because of their potential applications in molecular encapsulation,[17] drug delivery,[18] and nanoscopic transport.[19] The "unimolecular micelles" as termed by Newkome[20] have been made by modifying dendrimers with long hydrophobic or hydrophilic chains at their periphery, which can serve as a "dendritic box" for the encapsulation and transport of lipophilic compounds.[21] Percec and co-workers[23] reported that various self-assemblies can be formed by using different generation dendrons as building blocks. The molecular architectures can be designed from a disklike shape to cylindrical columns by the peripheral modification with lipophilic chains.[23] Meijer and co-workers[6,22] synthesized the poly(propylene imine) dendrimers with hydrophobic alkyl chains at their periphery, which form various self-assemblies from a globular inverted micellar arrangement to a cylindrical amphoteric structure. As mentioned above, much work has been devoted to the studies of the amphiphilic dendrimers bearing long soft chains at their periphery. However, little attention was paid to the aggregation behavior of the flexible hydrophilic dendrimers with rigid hydrophobic periphery.

In this article, we describe the peripheral modification of PAMAM dendrimers with naphthyl, pyrenyl, phenyl, and dansyl chromophores (Scheme 1). Their spectroscopic behavior has been explored with the aid of a series of small molecular model compounds. The aggregation and self-assembly of the hydrophilic PAMAM dendrimers bearing hydrophobic aromatic chromophores at their periphery have been observed and investigated systematically. To the best of our knowledge, this is the first report on the self-organization of the hydrophilic dendritic backbone with rigid hydrophobic periphery to form ordered aggregates.

Experimental Section

Materials, measurements, synthesis, and characterization of model compounds, i.e., *N*-(*N*′-1-naphthylsuccinimido)isobutylamine (MNp), *N*-(*N*′-1-pyrenylsuccinimido)isobutylamine (MPy), *N*,*N*-bis(*N*′-1-naphthylsuccinimido)isobutylamine (BNp), *N*,*N*-bis(*N*′-1-pyrenylsuccinimido)isobutylamine (BPy), were provided in the Supporting Information.

TEM and AFM Measurements. Transmission electron microscopic (TEM) measurement was performed on a JEM-100 CXII microscope,

(14) Baker, L. A.; Crooks, R. M. *Macromolecules* **2000**, *33*, 9034−9039.
(15) (a) Kopelman, R.; Shortreed, M.; Shi, Z. Y.; Tan, W. H.; Xu, Z. F.; Moore, J. S.; BarHaim, A.; Klafter, J. *Phys. Rev. Lett.* **1997**, *78*, 1239−1242. (b) Swallen, S. F.; Zhu, Z. G.; Moore, J. S.; Kopelman, R. *J. Phys. Chem. B* **2000**, *104*, 3988−3995. (c) Devadoss, C.; Bharathi, P.; Moore, J. S. *J. Am. Chem. Soc.* **1996**, *118*, 9635−9644. (d) Stewart, G. M.; Fox, M. A. *J. Am. Chem. Soc.* **1996**, *118*, 4354−4360. (e) Devadoss, C.; Bharathi, P.; Moore, J. S. *Macromolecules* **1998**, *31*, 8091−8099.
(16) (a) Serin, J. M.; Brousmiche, D. W.; Frechet, J. M. J. *J. Am. Chem. Soc.* **2002**, *124*, 11848−11849. (b) Frechet, J. M. J. *Proc. Natl. Acad. Sci. U.S.A.* **2002**, *99*, 4782−4787.
(17) (a) Niu, Y. H.; Crooks, R. M. *Chem. Mater.* **2003**, *15*, 3463−3467. (b) Nierengarten, J. F. *Top. Curr. Chem.* **2003**, *228*, 87−110. (c) Zimmerman, S. C.; Lawless, L. J. *Top. Curr. Chem.* **2001**, *217*, 95−120.
(18) Aulenta, F.; Hayes, W.; Rannard, S. *Eur. Polym. J.* **2003**, *39*, 1741−1771.
(19) Stiriba, S. E.; Frey, H.; Haag, R. *Angew. Chem., Int. Ed.* **2002**, *41*, 1329−1334.
(20) Newkome, G. R.; Moorefield, C. N.; Baker, G. R. *Angew. Chem., Int. Ed.* **1991**, *30*, 1178−1180.
(21) Narayanan, V. V.; Newkome, G. R. *Top. Curr. Chem.* **1998**, *197*, 19−77.
(22) (a) Schenning, A. P. H. J.; Elissen-Roman, C.; Weener, J. W.; Baars, M. W. P. L.; van der Gaast, S. J.; Meijer, E. W. *J. Am. Chem. Soc.* **1998**, *120*, 8199−8208. (b) Stevelmans, S.; van Hest, J. C. M.; Jansen, J. F. G. A.; van Boxtel, D. A. F. J.; de Brabander-van den Berg, E. M. M.; Meijer, E. W. *J. Am. Chem. Soc.* **1996**, *118*, 7398. (c) Bosman, A. W.; Janssen, H. M.; Meijer, E. W. *Chem. Rev.* **1999**, *99*, 1665−1688.
(23) (a) Percec, V.; Glodde, M.; Bera, T. K.; Miura, Y.; Shiyanovskaya, I.; Singer, K. D.; Balagurusamy, V. S. K.; Heiney, P. A.; Schnell, I.; Rapp, A.; Spiess, H. W.; Hudson, S. D.; Duan, H. *Nature* **2002**, *419*, 384−387. (b) Percec, V.; Ahn, C. H.; Cho, W. D.; Jamieson, A. M.; Kim, J.; Leman, T.; Schmidt, M.; Gerle, M.; Moller, M.; Prokhorova, S. A.; Sheiko, S. S.; Cheng, S. Z. D.; Zhang, A.; Ungar, G.; Yeardley, D. J. P. *J. Am. Chem. Soc.* **1998**, *120*, 8619−8631. (c) Hudson, S. D.; Jung, H. T.; Percec, V.; Cho, W. D.; Johansson, G.; Ungar, G.; Balagurusamy, V. S. K. *Science* **1997**, *278*, 449−452.

operating at an acceleration voltage of 100 kV. For the observation of size and distribution of vesicle particles, a drop of sample solution (concentration: 0.5 mg/mL) was placed on carbon-coated Formvar copper grids. About 2 min after the deposition, the grid was tapped with filter paper to remove surface water and air-dried. Negative staining was performed by addition of a drop of 2 wt % solution of uranyl acetate. An atomic force microscope (AFM, Dimension 3000, Digital instrument) was used in the tapping mode according to the literature procedures.[24a] A drop of sample solution (concentration: 0.5 mg/mL) was placed on the mica surface. AFM measurement was performed after the surface water was volatilized naturally at room temperature.

PAMAM Dendrimers G0−5 Peripherally Modified with Phenyl Groups (PAMAM-Ph G0−5) PAMAM-Ph G1. Benzaldehyde (10 mL, 0.037 g, 3.08 mmol) was added to a methanol solution (50 mL) of the first generation PAMAM dendrimer G1 (0.50 g, 0.35 mmol) in the presence of anhydrous sodium sulfate (2.0 g). After the reaction at 60 °C for 12 h under stirring, the system was cooled to room temperature and the solvent was removed under a reduced pressure. The residue was dissolved again in chloroform (5 mL). The solvent and excess benzaldehyde were removed under reduced pressure. The resulting yellow semisolid crude product was purified by repeated dissolution in methanol (5 mL) and precipitation in anhydrous diethyl ether (100 mL) with vigorous stirring. The precipitate was collected and further purified by dialysis using a dialysis membrane ($M_W = 1000$) to afford final product (0.1 g). Yield: 39%. FT-IR: (KBr pellet, cm^{-1}) 3278, 3061, 2936, 2841, 1645, 1552, 1450, 1378, 1254, 757, 720, 695. ^{1}H NMR ($CDCl_3$, TMS, ppm): δ7.36−7.66 (40H, aromatic ring), δ8.25 (8H, s, 8-CH═N−), δ3.67 (16H, 8-CH_2−CH_2−N═CH−), δ3.50 (16H, 8-NH−CH_2−CH_2−N═C−), δ3.18 (8H, 4-NH−CH_2−CH_2−N(−CH_2−)−CH_2−), δ2.65 (22H, 11-CH_2−N(−CH_2−)−CH_2−CH_2−), δ2.46 (12H, 6-CH_2−N(−CH_2−)−CH_2−), δ 2.25 (24H, 12-CH_2−CO−). ^{13}C NMR ($CDCl_3$, ppm): 172.49, 162.91, 135.69, 130.83, 128.56, 128.07, 60.24, 50.13, 40.13, 33.95. MALDI-TOF MS (matrix: dithranol/silver trifluoroacetate =1:1 w/w) calcd for $C_{118}H_{160}N_{26}O_{12}$ [M]: 2132. Found: 2133 (M + H $^+$), 2155 (M + Na^+).

PAMAM-Ph G0 and G2−5 were synthesized in the same manner as PAMAM-Ph G1. Their spectral characterization was provided in the Supporting Information. ^{1}H NMR spectra indicate that the reaction extent of the amino group (−NH_2) on the dendrimer surface with benzaldehyde was 90% for G0, 94% for G1, 92% for G2, 80% for G3, 85.7% for G4, and 88% for G5.

PAMAM Dendrimers G0−5 Peripherally Modified with Dansyl Chromophores (PAMAM-DNS G0−5) PAMAM-DNS G1. A methanol solution (20 mL) of PAMAM G1 (0.10 g, 0.070 mmol) was added dropwise to the aqueous solution (60 mL) of 5-(dimethylamino)-naphthalene-1-sulfonyl chloride (dansyl chloride) (0.151 g, 0.56 mmol) at room temperature for 40 min. The pH value of the reaction was kept between 10 and 12 by addition of an appropriate amount of NaOH aqueous solution (20 wt %). Then, the reaction was heated to 35 °C with stirring for 1 h. After evaporating the solvent under a reduced pressure, the residue was dissolved in methanol (5 mL), which was then dropped into anhydrous diethyl ether (100 mL) under stirring. A white precipitation was collected by suction filtration. The product was dissolved in methanol (10 mL) and dialyzed in a dialysis bag (M_W 1000) using methanol as a solvent at room temperature for 24 h. After evaporating methanol under reduced pressure and drying in a vacuum oven at 40 °C for 24 h, a pale yellow powder (0.05 g) was obtained. Yield: 23%. ^{1}H NMR: ($CDCl_3$, ppm) δ6.984−8.528 (48H, aromatic ring), δ2.763 (56H, 28-CH_2−N(−CH_2−)−CH_2−CH_2−)$_2$, δ3.481 (24H, 12-CH_2−NH−SO_2−), δ3.185 (48H, 8-N(CH_3)$_2$), δ2.534 (28H, 14-CH_2−CO−). IR (KBr pellet, cm^{-1}): 3078, 3480, 3360, 2849, 1647, 1542, 1456, 1318, 1324, 790. ^{13}C NMR ($CDCl_3$, ppm): 174.94, 155.28, 141.74, 132.22, 126.91, 123.17, 112.08, 50.33, 44.46, 35.35. MALDI-TOF MS (matrix: 2,5-dihydroxybenzoic acid) Calcd for $C_{159}H_{220}N_{34}O_{28}S_8$ [M]: 3302.4. Found: 3302 $(M)^+$.

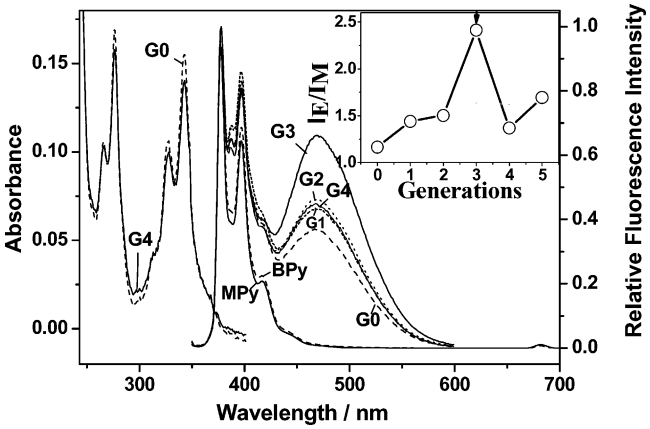

Figure 1. Absorption and emission spectra of PAMAM-Py G0−5 and mono- and bis-substituted model compounds MPy and BPy in dichloromethane. [Py] = 2.5×10^{-6} M. The emission spectra are normalized to the intensity at 378 nm. λ_{ex} = 335 nm. Inset: Variation of the pyrene I_E/I_M ratio with generations in dichloromethane. [Py] = 2.5×10^{-6} M.

PAMAM-DNS G0 and G2−5 were synthesized in the same manner as PAMAM-DNS G1. Their characterization was provided in the Supporting Information. ^{1}H NMR spectra indicated that the reaction extent of amino group (−NH_2) on the dendrimer surface with dansyl chloride was 90% for G0, 92% for G1, 90% for G2, 86% for G3, 86% for G4, and 80% for G5.

PAMAM Dendrimers G0−5 Peripherally Modified with Pyrenyl Chromophores (PAMAM-Py G0−5) PAMAM-Py G1. A methanol solution (25 mL) of PAMAM G1 (0.0136 g, 0.00952 mmol) was added dropwise to an acetone solution (30 mL) of *N*-(1-pyrenyl)maleimide (0.050 g, 0.168 mmol) at 0 °C. The resultant solution was kept at 30 °C with stirring for 48 h. After evaporating the solvent under a reduced pressure, the residue was dissolved in methanol (5 mL), which was then dropped into anhydrous diethyl ether (100 mL) with stirring. A white precipitation was collected by suction filtration, then dissolved again in methanol (10 mL) and dialyzed with a dialysis bag (M_W 3500) using methanol as a solvent at room temperature for 24 h. After evaporating methanol under a reduced pressure and drying in a vacuum oven at 40 °C for 24 h, a pale yellow powder (0.0070 g) was obtained. Yield: 30%. IR (KBr pellet, cm^{-1}): 3021, 3116, 2925, 1641, 1504, 1411, 1326, 781, 735. ^{1}H NMR: ($CDCl_3$, ppm) δ7.597−8.235 (72H, aromatic ring), δ3.700 (8H, 8-CH_2−C*H* (−CO−)−NH−), δ2.873 (16H, 8-NH−CH_2−CH_2−N(−CH_2−)−CH_2−), δ3.483 (16H, 8-CH_2−CH_2−NH−CH(−CO−)−CH_2−), δ3.323 (8H, 4-NH−CH_2−CH_2−NH−CH−), δ2.654 (32H, 16-CH_2−N(−CH_2−)−CH_2−CH_2−), δ2.366 (24H, 12-CH_2−CO−). MALDI-TOF MS (matrix: 2,5-dihydroxybenzoic acid) Calcd for $C_{223}H_{220}N_{34}O_{28}$ [M]: 3821.7. Found: 3846 (M + Na)$^+$.

PAMAM-Py G0 and G2−5 were synthesized in the same manner as PAMAM-Py G1. Their spectral characterization was provided in the Supporting Information. ^{1}H NMR spectra indicated that the reaction extent of amino group (−NH_2) on the dendrimer surface with *N*-(1-pyrenyl)maleimide was 95% for G0, 65% for G1, 95% for G2, 98% for G3, 73% for G4, and 90% for G5.

PAMAM dendrimers G0−5 with terminal mono- and bis-naphthyl chromphores (PAMAM-MNp G0−5 and PAMAM-BNp G0−5) were synthesized in a similar manner as PAMAM-Py G1 except for the starting materials. Their spectral characterization was provided in the Supporting Information. ^{1}H NMR spectra indicated that the reaction

(24) (a) Wang, J. F.; Jia, X. R.; Zhong, H.; Luo, Y. F.; Zhao, X. S.; Cao, W. X.; Li, M. Q. *Chem. Mater.* **2002**, *14*, 2854−2858. (b) Fluorescence quantum yields were calculated from the integrated intensity under the emission band *A* using the following equation: $\phi = \phi_r(A/A_r)(OD_r/OD)(n^2/n_r^2)$, where OD is the optical density of the solution at the excitation wavelength, and *n* is the refractive index. The optical density of the solution for the calculation of quantum yields was less than 0.1 at the excitation wavelength. The solvent 9,10-diphenylanthrene in cyclohexane was used as reference ($\phi_r = 0.90$) (Eaton, D. F. *Pure Appl. Chem.* **1988**, *60*, 1107−1114.)

extents of amino group ($-NH_2$) on the dendrimer surface with *N*-(1-naphthyl) maleimide were 93.5%, 83%, 89%, 95%, 70%, and 83% for PAMAM-MNp G0−5, respectively, and 90%, 92%, 90%, 86%, 86%, and 76% for PAMAM-BNp G0−5, respectively.

Results and Discussion

Absorption and Fluorescence Spectroscopy. A. Model Compounds. To better understand the spectroscopic properties of the peripherally aromatic-modified dendrimers, a series of mono- and bis-substituted model compounds, i.e., MPy, BPy, MNp, and BNp, were synthesized by controlling the feed radios in a Michael addition of isobutylamine with *N*-(1-naphthyl)-maleimide or *N*-(1-pyrenyl)maleimide.

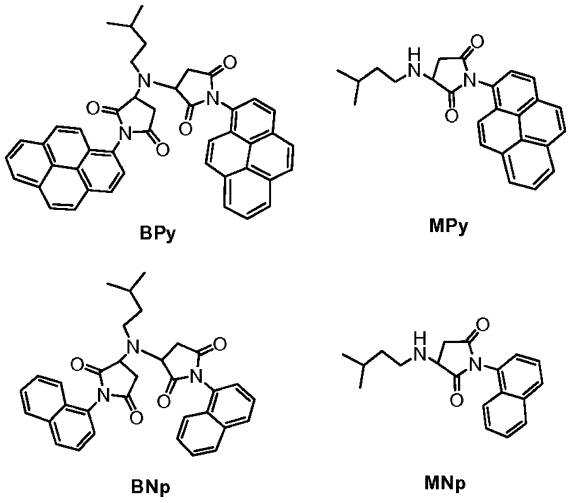

The absorption and emission spectra of BPy and MPy display the same peak shape and position as shown in Figure 1. The fluorescence quantum yield (Q)[24b] and lifetime (τ) of BPy ($Q = 0.120$ and $\tau = 72.6$ ns) are about 2 times larger than those of MPy ($Q = 0.0592$ and $\tau = 29.5$ ns). This may be attributed to a sharp increase in the molecular rigidity of BPy due to the steric crowding of two pyrene rings.

For MNp and BNp, their absorption and emission spectra do not exhibit a significant difference. The fluorescence quantum yield and lifetime of BNp ($Q = 0.203$ and $\tau = 7.81$ ns) are slightly higher than those of MNp ($Q = 0.199$ and $\tau = 7.78$ ns), suggesting that the two naphthyl rings of BNp do not lead to a large increase in molecular rigidity as BPy. In addition, it was found that the bis-substituted model compounds BPy and BNp do not show excimer fluorescence, implying that two pyrene or naphthalene rings may not form an intramolecular parallel geometric arrangement. A conformational analysis of the energy minimum of BPy and BNp (calculated with a semiempirical AM1 method using a Gaussian98 program) also reveals that the two pyrene or naphthalene rings are not parallel but almost perpendicular to each other with twist angles of 76.1° and 93.4°, respectively.

B. PAMAM Dendrimers G0−5 Peripherally Modified with Pyrenyl Chromophore (PAMAM-Py G0−5). Figures 1, 3, and 4 show the absorption and emission spectra of the dendrimers of the zeroth to fifth generations peripherally modified with aromatic chromophores. For these dendrimers, there is little peak broadening or shift in the absorption spectra with increasing generation, suggesting that these peripheral chromophores are well separated with very weak electron coupling in their ground state. However, in sharp contrast, their fluorescence spectra are quite different.

For PAMAM-Py G0−5, a broad structureless fluorescence peak was observed at 468 nm, which is well-known to be attributable to the formation of $\pi-\pi$ interaction between adjacent parallel-oriented pyrene chromophores. The excimer emission increases from G0 to G3 as shown in Figure 1, suggesting that the higher generations favor the parallel arrangement between peripheral pyrene rings. However, the excimer fluorescence of PAMAM-Py G4 and G5 has lower intensities than that of the third generation. This may be due to the fact that the peripheral chromophores of the fourth and fifth generations (G4 and G5) are more sterically crowded, which in turn prevents the pyrene rings from parallel arrangement.

Such a fluorescence behavior is further quantified using a widely applied fluorescence intensity ratio (I_E/I_M) method according to Winnik et al..[25] The intensity ratio (I_E/I_M) was calculated by taking the ratio of the integrals under the fluorescence band of 435−555 nm for the pyrene excimer (I_E) to that of 372−435 nm for the pyrene monomer (I_M). The inset of Figure 1 shows that the I_E/I_M value increases and reaches a maximum at the third generation, suggesting that the parallel arrangement is optimized at the third generation. In addition, the I_E/I_M ratios were found to not depend on the dendrimer concentration, indicating that the formation of pyrene excimer is due to an intramolecular process of the dendrimers. These results manifest the strong effect of dendritic architectures on the fluorescence spectra. According to Tomalia,[26a] Turro,[26b] Goddard,[26c] and Zimmerman,[27] the lower generations of dendrimers are highly asymmetric and tend to exist in an open and extended form; in contrast, the higher generations adopt a three-dimensional globular structure with a densely packed chromophore shell. Therefore, further analysis of the changes in the I_E/I_M value reveals an extended-to-globular architectural transition occurring at the third generation.

It is very interesting to note that our results are slightly different from those reported by Crooks and Baker for poly(propylene imine) dendrimers with a peripheral pyrene chromophore.[14] In their system, the excimer emission of pyrene increases continuously from G2 to G5. The highest generation G5 displays the strongest excimer emission. Such a difference could be readily rationalized by considering the difference in the dendritic backbones. The excimer formation is known to be strongly affected by its initial excited-state placement within the dendrimer framework according to Moore and co-workers.[15b] In our system, PAMAM dendrimer is relatively more rigid because of the internal H-bonding interactions as compared with the poly(propylene imine) in Crooks' system. At the fourth and fifth generations, PAMAM dendrimer may not be flexible enough to effectively optimize the parallel arrangement of pyrene rings.

To develop a better understanding of the fluorescence behavior of PAMAM-Py, the fluorescence decay was measured by using a time-correlated single-photon counting technique.

(25) (a) Winnik, F. M.; Regismond, S. T. A. *Colloids Surf., A* **1996**, *118*, 1−39. (b) Winnik, F. M. *Chem. Rev.* **1993**, *93*, 587−614. (c) Capek, I. *Adv. Colloid Interface Sci.* **2002**, *97*, 91−149.
(26) (a) Tomalia, D. A.; Naylor, A. M.; Goddard, W. A. *Angew. Chem., Int. Ed.* **1990**, *29*, 138−175. (b) Caminati, G.; Turro, N. J.; Tomalia, D. A. *J. Am. Chem. Soc.* **1990**, *112*, 8515. (c) Naylor, A. M.; Goddard, W. A. *J. Am. Chem. Soc.* **1989**, *111*, 2339.
(27) Zeng, F. W.; Zimmerman, S. C. *Chem. Rev.* **1997**, *97*, 1681−1712.

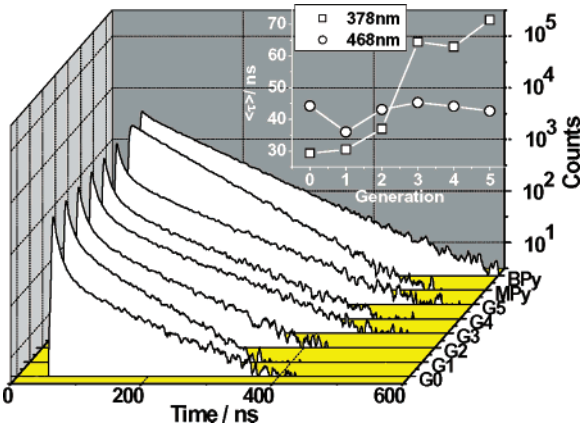

Figure 2. Fluorescence decay curves of PAMAM-Py G0−5 and mono- and bis-substituted model compounds MPy and BPy in dichloromethane. [Py] = 2.5×10^{-6} M. λ_{ex}= 335 nm. λ_{em}= 378 nm. Inset: Average fluorescence lifetimes $\langle\tau\rangle$ of pyrenyl monomer and excimer of PAMAM-Py G0−5 in dichloromethane at the emission wavelengths of 378 and 468 nm, respectively. λ_{ex} = 335 nm.

Figure 2 shows that the average fluorescence lifetimes $\langle\tau\rangle$[28] of monomeric pyrene emission of PAMAM-Py at 378 nm increase with increasing generation. A rapid rise in the lifetime was found from G2 to G3 as shown in the inset of Figure 2, implying a sharp increase in molecular rigidity from G2 to G3. This observation further supports the assertion that the extended-to-globular transition of dendritic architecture occurs between G2 and G3. Compared with the model compounds MPy and NPy, the average fluorescence lifetimes and quantum yields of PAMAM-Py G0−5 are generally lower. This could be attributed to the quenching effect of amidoamine branches of PAMAM dendrimers according to Pistolis and co-workers.[29] However, the average lifetimes of the pyrene excimer emission at 468 nm do not have a simple correlation with generation as shown in the inset of Figure 2.

C. PAMAM Dendrimers G0−5 with Terminal Mono- and Bis-naphthyl Chromophores (PAMAM-MNp G0−5 and PAMAM-BNp G0−5). Figure 3 shows the absorption and emission spectra of the dendrimers bearing peripheral naphthyl chromophores PAMAM-MNp G0−5. There is a typical emission band of naphthyl group at 335 nm. No excimer emission was observed for these dendrimers at all generations. The result is consistent with that reported for polyether dendrons with naphthyl chromophores by Fox and Stewart.[15d]

The inset of Figure 3 shows the fluorescence quantum yields[24] of PAMAM-MNp and PAMAM-BNp G0−5. Time-resolved fluorescence measurements indicate that the average fluorescence lifetimes[28] of PAMAM-MNp G0−5 are 5.26, 4.67, 1.19, 5.15, 5.28, and 3.68 ns, respectively. PAMAM-MNp G2 exhibits the lowest quantum yield and fluorescence lifetime at all generations. This may arise from two factors: (1) As the generation increases, the torsional and rotational mobility of the naphthyl group was hindered to cause an increase in molecular rigidity, which thus results in an increased quantum yield. (2) The amidoamine branches of dendritic backbone are known to have a fluorescence quenching effect.[29] These two factors lead to the lowest quantum yields for PAMAM-MNp G2, where the relatively rigid and globular structures are not yet formed, and the fluorescence quenching of dendritic backbone dominates. For the dendrimers with terminal bis-naphthyl chromophores PAMPAM-BNp G0−5, their quantum yields do not depend on the generations as shown in the inset of Figure 3. The weak or negligible effect of dendritic architectures may be due to the fact the peripheral adjacent naphthyl groups are always close to each other at all generations of PAMAM-BNp. For PAMAM-Ph G0−5, their fluorescence is too weak to warrant a meaningful quantitative analysis.

D. PAMAM Dendrimers G0−5 Peripherally Modified with Dansyl Chromophores (PAMAM-DNS G0−5). The above dendrimers possess nonpolar naphthyl, pyrenyl groups at their periphery. The emission behavior of these aromatic chromophores is not sensitive to their surrounding polarity. In contrast, it is well-known that, in the case of the polar dansyl group, its emission position, shape, and intensity are sensitive to local hydrophobicity, mobility, solvation, polarity, viscosity, and free volume as well as H^+ ion concentration (pH) according to Vögtle and co-workers.[7,30] To further explore the relationship between dendrimer architectures and spectroscopic behavior, we peripherally modified the PAMAM dendrimer G0−5 with polar dansyl chromophores and investigated their fluorescence behavior. Figure 4 shows the emission spectra of PAMAM-DNS G0−5. Interestingly, the fluorescence emission at a shorter wavelength of about 413−450 nm decreases gradually, and the emission at a longer wavelength of about 512 nm increases with increasing generation. The second and third generations display dual fluorescence bands at about 448 and 512 nm.

The dansyl group is a typical twisted intramolecular charge transfer (TICT) fluorophore according to Rettig and co-workers.[31] When the dansyl group is located in a nonpolar or hydrophobic microenvironment, the dimethylamino moiety mostly takes a coplanar conformation with the naphthyl group at the excited state, which is termed as a locally excited (LE) state. The maximum emission wavelength of the LE state is about 430 nm. When the dansyl group is located in a polar or hydrophilic microenvironment, the dimethylamino moiety mostly takes a twisted conformation with the naphthyl group at the excited state to form a twisted intramolecular charge transfer (TICT) state. The maximum emission wavelength of the TICT state is about 520 nm.[25c]

Figure 4 shows a spectral shift and transform from about 445 nm to 512 nm in the same solvent with increasing generations, implying that the coplanar LE state was gradually converted to a TICT excited state from the low to the higher generations. In

(28) Average decay time $\langle\tau\rangle$ was calculated from the following equation:

$$\langle\tau\rangle = \sum_{i=1}^{k} A_i \tau_i \Big/ \sum_{i=1}^{k} A_i$$

The parameters of the fits were optimized by using the Marquardt−Levenberg algorithm. Press, W. H.; Flannery, B. P.; Teukolsky, S. A.; Vetterling, W. E. T. *Numerical Recipes. The Art of Scientific Computing-(Fortran Version)*; Cambridge University Press: New York, 1992. The quality of the fits was estimated from the χ^2, the residuals, and the autocorrelation function of the residuals.

(29) Pistolis, G.; Malliaris, A.; Paleos, C. M.; Tsiourvas, D. *Langmuir* **1997**, *13*, 5870−5875.

(30) (a) Vögtle, F.; Gestermann, S.; Kauffmann, C.; Ceroni, P.; Vicinelli, V.; Balzani, V. *J. Am. Chem Soc.* **2000**, *122*, 10398−10404. (b) Vögtle, F.; Gestermann, S.; Kauffmann, C.; Ceroni, P.; Vicinelli, V.; de Cola, L.; Balzani, V. *J. Am. Chem. Soc.* **1999**, *121*, 12161−12166.

(31) (a) Grabowski, Z. R.; Rotkiewicz, K.; Rettig, W. *Chem. Rev.* **2003**, *103*, 3899−4031. (b) Rettig, W.; Strehmel, B.; Schrader, S.; Seifert, H. *Applied Fluorescence in Chemistry, Biology and Medicine*; Springer-Verlag: Berlin, 1999. (c) Rettig, W.; Lapouyade, R.; Lakowicz, J. R. *Topic In Fluorescence Spectroscopy. Volume 4: Probe Design and Chemical Sensing.* Plenum Press: New York, 1994; pp 109−149. (d) Maus, M.; Rettig, W.; Bonafoux, D.; Lapouyade, R. *J. Phys. Chem. A* **1999**, *103*, 3388−3401.

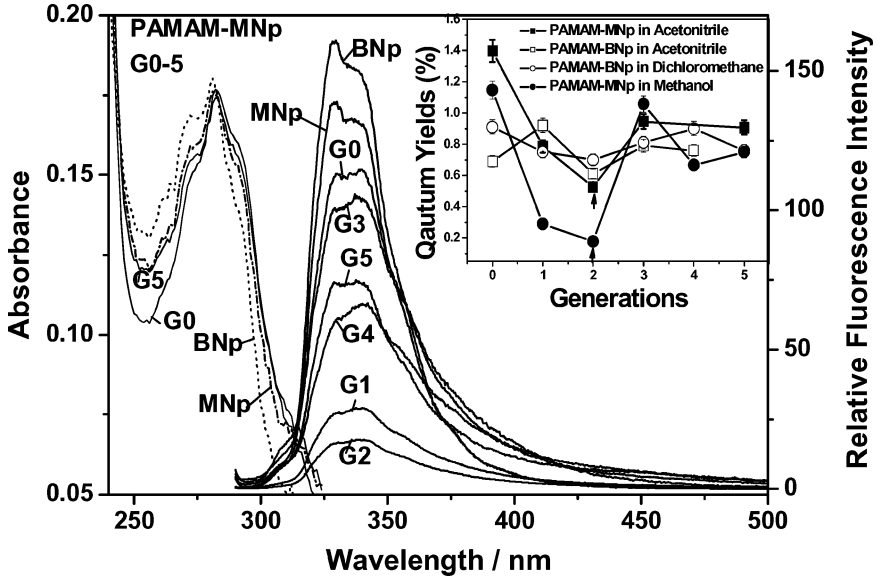

Figure 3. Absorption and emission spectra of PAMAM-MNp G0−5 as well as mono- and bis-substituted model compounds MNp and BNp. The spectra are normalized to the naphthyl chromophore concentration of 0.5×10^{-5}M. Inset: Fluorescence quantum yields of PAMAM-BNp and PAMAM-MNp G0−5 in methanol, acetonitrile, and dichloromethane.

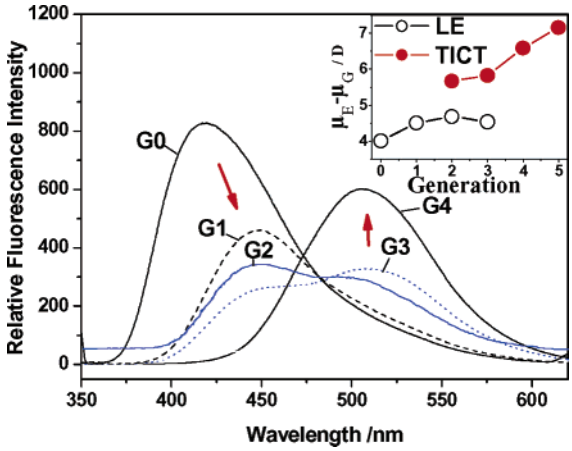

Figure 4. Fluorescence emission spectra of PAMAM-DNS G0−5 in CH_2Cl_2 at the concentration 0.5×10^{-5} M. Inset: Changes in dipole moment of the ground (μ_G) and excited states (μ_E) of dansyl groups at the different generations.

other words, the changes in dendritic architecture induce the conversion between the two excited states. At the second and third generations, where the extended-to-globular transition occurs, the observation of dual fluorescence bands suggests the coexistence of the coplanar LE and twisted TICT excited states. The conversion from the LE to TICT state can be reasonably explained as follows: At the higher generations, the conformation of the dansyl group tends to be slightly twisted due to the steric crowding at the ground state. Upon photoexcitation, the pretwisted conformation readily leads to a TICT excited-state according to Rettig et al..[31a,d]

In principle, the fluorescence behavior in various solvents can reflect the changes in the excited state of chromophores, which can be described quantitatively by Lippert equation[32] as follows,

$$\nu_a - \nu_f = (2/hc)(\Delta f)[(\mu_E - \mu_G)^2/a^3] + \text{constant} \qquad (1)$$

where ν_a and ν_f are the wavenumbers (cm^{-1}) of the absorption and emission, respectively; μ_G and μ_E are the dipole moment of ground state and excited state, respectively; Δf is a solvent parameter termed as the orientation polarizability.[33]

According to the Stokes' shift ($\Delta\nu = \nu_a - \nu_f$) in polar and nonpolar solvent (Δf),[33] the value $(2/hc)[(\mu_E - \mu_G)^2/a^3]$ was determined from the slope of the plot of $\Delta\nu$ against Δf using eq 1. On the basis of the Onsager cavity radius ($a = 0.366$ nm) of the dansyl group as reported by Letard and Rettig,[34] the changes ($\Delta\mu = \mu_E - \mu_g$) in dipole moments between the first excited singlet state and the ground state were obtained as shown in the inset of Figure 4. There is a trend that the $\Delta\mu$ increases from G0 (4.01 D) to G3 (4.54 D) for the coplanar LE state. For the TICT excited state of higher generations, the same trend was observed from G2 (5.67 D) to G5 (7.16 D), which displays a larger change in dipole moment than the coplanar LE state. It should be noted that one Debye unit (1.0 D) is 1×10^{-18} esu cm, and 5.67 D is comparable to the dipole moment that results from a charge separation of one unit charge (4.8×10^{-10} esu) by 1.18 Å. These data are close to $\Delta\mu = 5.48$ D for 5-(dimethylamino)naphthalene-1-sulfonic acid [2-(vinyloxy-methylamino)ethyl]amide reported by Ren and Tong[35] and $\Delta\mu = 5.78$ D for dansyl-monoaza-18-crown-6 reported by Wu and co-workers.[36] From these results, it is reasonable to conclude that the dendritic architectures at different generations have a strong influence on the excited state of peripheral dansyl chromophores.

Fluorescence Quenching. To gain further insights into the effect of dendritic architectures, we investigated the fluorescence

(32) Lakowicz, J. R. *Principles of Fluorescence Spectroscopy*, 2nd ed.; Plenum Press: New York, 1999; p 239.

(33) Solvent parameters (Δf) of tetrahydrofuran, dichoromethane, *N*,*N*-dimethylformamide, methanol, and acetonitrile were calculated to be 0.2097, 0.2183, 0.2755, 0.3085, and 0.3054, respectively, according to the equation $\Delta f = (\epsilon - 1)/(2\epsilon + 1) - (n^2 - 1)/(2n^2 + 1)$, where ϵ and n are the dielectric constant and refractive index of solvents, respectively.

(34) Letard, J. F.; Lapouyade, R.; Rettig, W. *Pure Appl. Chem.* **1993**, *65*, 1705−1712.

(35) Ren, B. Y.; Gao, F.; Tong, Z.; Yan, Y. *Chem. Phys. Lett.* **1999**, *307*, 55−61.

(36) Wu, Y.; Li, L.; Tong, A. *Chin. Sci. Technol. Lett.* **1998**, *4*, 196−197.

Table 1. Stern−Volmer Constants ($k_q\tau_0$) and Bimolecular Quenching Constants (k_q) of the Fluorescence Quenching of PAMAM-Py G0−5 by *N*,*N*-Dimethylphenylamine and PAMAM-BNp G0−G5 and PAMAM-MNp G0−5 by Triethylamine

PAMAM-Py						
	G0	G1	G2	G3	G4	G5
$K_q\tau_0/M^{-1}$	35.9	30.8	31.68	17.22	53.45	24.4
$k_q/M^{-1}\ s^{-1}\ (10^9)$	1.225	1.01	0.86	0.27	0.85	0.34
PAMAM-BNp						
	G0	G1	G2	G3	G4	G5
$k_q\tau_0/M^{-1}$	121	53.9	51.0	179.0	176.0	180.0
$k_q/M^{-1}\ s^{-1}\ (10^9)$	23.1	11.5	6.56	34.4	33.3	48.9
PAMAM-MNp						
	G0	G1	G2	G3	G4	
$k_q\tau_0/M^{-1}$	329	186	182	52	74	
$k_q/M^{-1}\ s^{-1}\ (10^9)$	62.6	39.8	23.4	10.0	14.0	

quenching of PAMAM-Py by *N*,*N*-dimethylphenylamine and PAMAM-MNp and PAMAM-BNp by triethylamine. The kinetics of steady-state fluorescence quenching is described by the Stern−Volmer equation:[32] $I_0/I = 1 + k_q\tau_0[Q]$, where I_0 and τ_0 are the unquenched intensity and lifetime, and [Q] is the quencher's concentration. The quenched intensity (I) was corrected to avoid the inner filter effects due to the absorption of quenchers.[37a] It is important to note that the correction for the quenched intensity is very necessary when the absorption of quenchers is close to the excitation wavelength. Some unreasonable results (e.g., $k_q \gg 10^{10}\ M^{-1}\ s^{-1}$) would be readily obtained if the data were not corrected.[37b,c] The Stern−Volmer plots for the fluorescence quenching were given in the Supporting Information. The Stern−Volmer constant ($k_q\tau_0$) and bimolecular quenching constant (k_q) were summarized in Table 1.

In principle, k_q reflects the quenching efficiency or the accessibility of the quenchers to the fluorophore.[32] The k_q values for the zeroth generation PAMAM-MNp, PAMAM-BNp, and PAMAM-Py are close to $10^{10}\ M^{-1}\ s^{-1}$, indicating a diffusion-controlled quenching. This suggests that the dendrimers of low generations have a more extended conformation, which is readily accessible to the quencher. With increasing generation from G0 to G3, the k_q value becomes smaller due to the steric effect. The third generation dendrimers tends to be globular in conformation, hence, more shielded from quenchers. The collisional dynamic quenching occurs only if the quenchers approach the peripheral fluorophores from a particular direction. At the higher generations, i.e., G4 and G5, the k_q value was found to be generally greater. In addition, at higher quencher concentrations, the I_0/I ratio deviated from the linear Stern−Volmer plot. A similar phenomenon was also observed by Moore and Devadoss.[15e] This can be well understood from the architectural effect. The globular architectures of G4 and G5 with a densely packed shell can encapsulate and bind the quencher molecules such as a "dendritic box" as described by Meijer,[38] which leads to an effective static quenching as illustrated in Figure 5.

Aggregation Behavior. A. Atomic Force and Transmission Electron Microscopy of the Dendrimer Assemblies. The peripherally aromatic modified PAMAM dendrimers with hydrophobic shell and hydrophilic aminoamine interior are expected to display an amphiphilic property. Therefore, the self-assembly of these amphiphilic dendrimers was studied by means of atomic force microscopy (AFM) and transmission electron microscopy (TEM). Figures 6 and 7 show the AFM and TEM images of PAMAM-Ph G0−2 assemblies in water. The spherical aggregates or vesicles of ca. 100 nm in diameter were observed. The aggregate size falls into the range of the typical vesicular size of traditional surfactants[39] and amphiphilic diblock copolymers (30−100 nm).[40]

Interestingly, a large number of multiple aggregates, i.e., "twins" and "quins" consisting of two and five individual aggregates, were observed for PAMAM-Ph G1 and G2, respectively, as shown in Figure 6b and c. The mechanism for the formation of these remarkable multiple aggregate "twins" and "quins" will be discussed in the following section. For higher generations G4 and G5, we did not observe the formation of any ordered aggregates in water.

Figure 7 compares the TEM images of PAMAM-Ph G1 aggregates with and without negative staining. It is clearly identifiable that the "twins" and "quins" aggregates possess a bilayer vesicular structure. The hydrophobic interphase of bilayer appears in gray due to the high electron density of aromatic chromophores before staining as shown in Figure 7b. After electron staining with uranyl acetate, an exactly reversed image was observed as shown in Figure 7a. The hydrophobic interphase of bilayer was shown as relatively lighter features. The other water-soluble portion appears in black because of the staining by uranyl acetate. In addition, it was found that most "twins" aggregates disappear after the staining as shown in Figure 7a, suggesting that the electron staining process may have an influence on the aggregate formation.

In contrast to the generally observed spherical vesicles, the PAMAM-Py dendrimers were found to self-organize into triangle-like vesicles in water (Figure 8). White striation could be clearly identified from TEM images, which corresponds to the hydrophobic interphase (l_h) between bilayers with a thickness of ca. 2.5 nm. Although the vesicles had a relatively thin wall and varied shapes, they are very stable as evidenced by the observation that the vesicular morphology exists over a considerably long time (~10 days). This may be attributed to the strong $\pi-\pi$ interaction of pyrene rings in hydrophobic part and H-bonding interactions in hydrophilic part of the dendrimers.

Figure 9 gives a representative TEM image of PAMAM-MNp G0 aggregates in water. The average sizes of PAMAM-MNp and PAMAM-BNp aggregates observed by AFM and TEM are listed in Table 3. It was found that the average diameter of these aggregates decreases gradually from G0 to G3. The thickness of hydrophobic interphase (l_h) directly observed from TEM is

(37) (a) To avoid the inner filter effects due to the absorption of the incident light and the emitted light, the fluorescence intensity was corrected as follow: $I = I_{obsd} \times 10^{[(OD_{ex}+OD_{em})/2]}$. I_{obsd} is the observed fluorescence intensity. OD_{ex} and OD_{em} are the optical densities at excitation and emission wavelength, respectively. (b) Phelan, J. C.; Sung, C. S. P. *Macromolecules* **1997**, *30*, 6845−6851. (c) Phelan, J. C.; Sung, C. S. P. *Macromolecules* **1997**, *30*, 6837−6844.

(38) Jansen, J. F. G. A.; de Brabander-van den Berg, E. M. M.; Meijer, E. W. *Science* **1994**, *266*, 1226−1229.

(39) (a) Marrink, S. J.; Mark, A. E. *J. Am. Chem. Soc.* **2003**, *125*, 15233−15242. (b) Myers, D. *Surfaces, Interfaces, and Colloids: Principles and Applications*, 2nd ed.; John Wiley & Sons: New York, 1999.

(40) (a) Discher, D. E.; Eisenberg, A. *Science* **2002**, *297*, 967−973. (b) Zhang, L. F.; Yu, K.; Eisenberg, A. *Science* **1996**, *272*, 1777−1779. (c) Zhang, L. F.; Eisenberg, A. *Science* **1995**, *268*, 1728−1731.

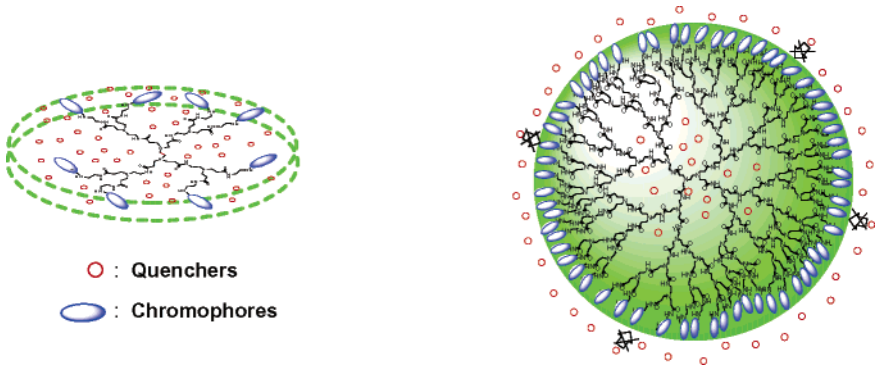

Figure 5. Schematic illustration for more extended architecture at low generations (e.g., G1) with an open and accessible structure by quenchers (left) and the globular architecture at higher generations (e.g., G4) with a densely packed shell (right). The closed globular structure could encapsulate and bind some quenchers in its interior but sterically hinder outer quenchers from entering into its interior.

in a range of 2.3−3.4 nm. The bilayer thickness in a range of 3.6−6.4 nm was thus obtained from the hydrophobic thickness (l_h) plus 2 times the maximum extended length of dendrimers (l_d). The data are close to the thickness of natural lipid membranes (∼5 nm) and the bilayer thickness (4.8−5.4 nm) of vesicles from poly(propylene imine) dendrimer bearing long hydrophobic soft chains reported by Meijer and Schenning.[22a] The bilayer thickness is much lower than those for the vesicles made from amphiphilic block copolymers (10−20 nm).[40] So far, there have been many vesicle-forming species reported such as hydrophilic modified fullerenes,[41a] cationic and anionic surfactants,[41b] and various amphiphilic block copolymers.[41c] To the best of our knowledge, this is the first observation of the bilayer vesicle formation from the hydrophilic dendrimers bearing short hydrophobic rigid chromophores at their periphery.

The formation of bilayer vesicles can be attributed to the amphiphilic structure of dendrimers, i.e., hydrophilic dendritic branches and hydrophobic aromatic periphery. At the low generations (G0−3), the open and extended architectures facilitate the changes in shapes of the dendrimers. The hydrophilic branches of dendrimers tumble out to occupy more room in water. To minimize the energy in water, the hydrophobic aromatic moieties of dendrimers shrink and pack together in parallel with the aid of $\pi-\pi$ interaction to form the hydrophobic interphase between bilayers as illustrated in Figure 10.

The bilayer structure of vesicles was clearly confirmed by their TEM images with and without negative staining (Figures 7, 8, and 11). The outer and inner layers of the vesicles appear in black from TEM images with negative staining, indicating that the portion consists of the hydrophilic dendritic branches. The bilayer interphase appears in relative gray from the TEM images without negative staining, indicating that the interphase consists of hydrophobic aromatic moieties with high electron density.

Because the flexible hydrophilic dendritic branches are located in the outer layer, these vesicles are very adhesive. They are readily attached by H-bonding interaction and the entanglement of the branches. Therefore, a large number of aggregate "twins" consisting of two vesicles, even multivesicle "quins" consisting of five individuals, were observed. Further fusion of two attached vesicles leads to the structures from "twins I" to "twins II" as shown in Figures 6c, 10, and 11.

In contrast to the vesicles from traditional amphiphilic compounds, these dendrimer-based vesicles have several distinct features. (1) They possess a very thin wall (hydrophobic interphase of 2.3−3.4 nm) as compared with the vesicles from diblock copolymers (10−20 nm). (2) The driving force for the self-organization may be the $\pi-\pi$ interaction of aromatic moieties and H-bonding interaction of dendrimer branches. (3) The driving force of self-organization along with further entanglement of the dendrimer branches leads to the formation of a large number of multivesicle "twins" and "quins" with a significant degree of internal stability.

For the fourth and fifth generations of these dendrimers, however, no ordered aggregates or vesicles were observed (Figure S-12 in the Supporting Information). This is expected due to the fact that the dendrimers G4 and G5 possess a globular architecture with a compact surface. The sterical crowding and rigid dendritic architecture are not flexible enough to form ordered assemblies. Recently, Meijer and Stevelmans[22] also reported the absence of the ordered superstructures at higher generations (e.g., G4 or higher).

B. Critical Aggregation Concentration, Aggregation Number, and Critical Packing Parameter. To further elucidate the mechanism for the aggregate formation, we have measured some key aggregation parameters. The critical aggregation concentration (CAC) of these dendrimer aggregates was determined by following the change in fluorescence intensity or the ratio (I_E/I_M) with increasing dendrimer concentration.[25,32] The original plots are shown in Figure S-8 in the Supporting Information. The CAC values obtained are summarized in Table 2.

All the CAC values are very low ($10^{-5}-10^{-7}$ M) as expected for these amphiphilic dendrimers. The CAC value appears to decrease in the order of PAMAM-MNp > PAMAM-BNp > PAMAM-Py. PAMAM-Py self-organizes into ordered aggregates more readily than PAMAM-BNp and PAMAM-MNp. This indicates that pyrene rings or larger aromatic chromophores favor the self-organization process due to the stronger $\pi-\pi$ interaction. In addition, the CAC value decreases gradually from G0 to G3, suggesting that the aggregates are favorably formed in the order of G3 > G2 > G1 > G0. Within the range of G0−3, the higher generations favor aggregation because of the increase in aromatic rings and dendrimer branches.

Currently, there are several techniques to obtain the information on the aggregate characteristics, such as a light scattering

(41) (a) Zhou, S. Q.; Burger, C.; Chu, B.; Sawamura, M.; Nagahama, N.; Toganoh, M.; Hackler, U. E.; Isobe, H.; Nakamura, E. *Science* **2001**, *291*, 1944−1947. (b) Wang, X. H.; Goh, S. H.; Lu, Z. H.; Lee, S. Y.; Wu, C. *Macromolecules* **1999**, *32*, 2786−2788. (c) Jung, H. T.; Coldren, B.; Zasadzinski, J. A.; Iampietro, D. J.; Kaler, E. W. *Proc. Natl. Acad. Sci. U.S.A.* **2001**, *98*, 1353−1357.

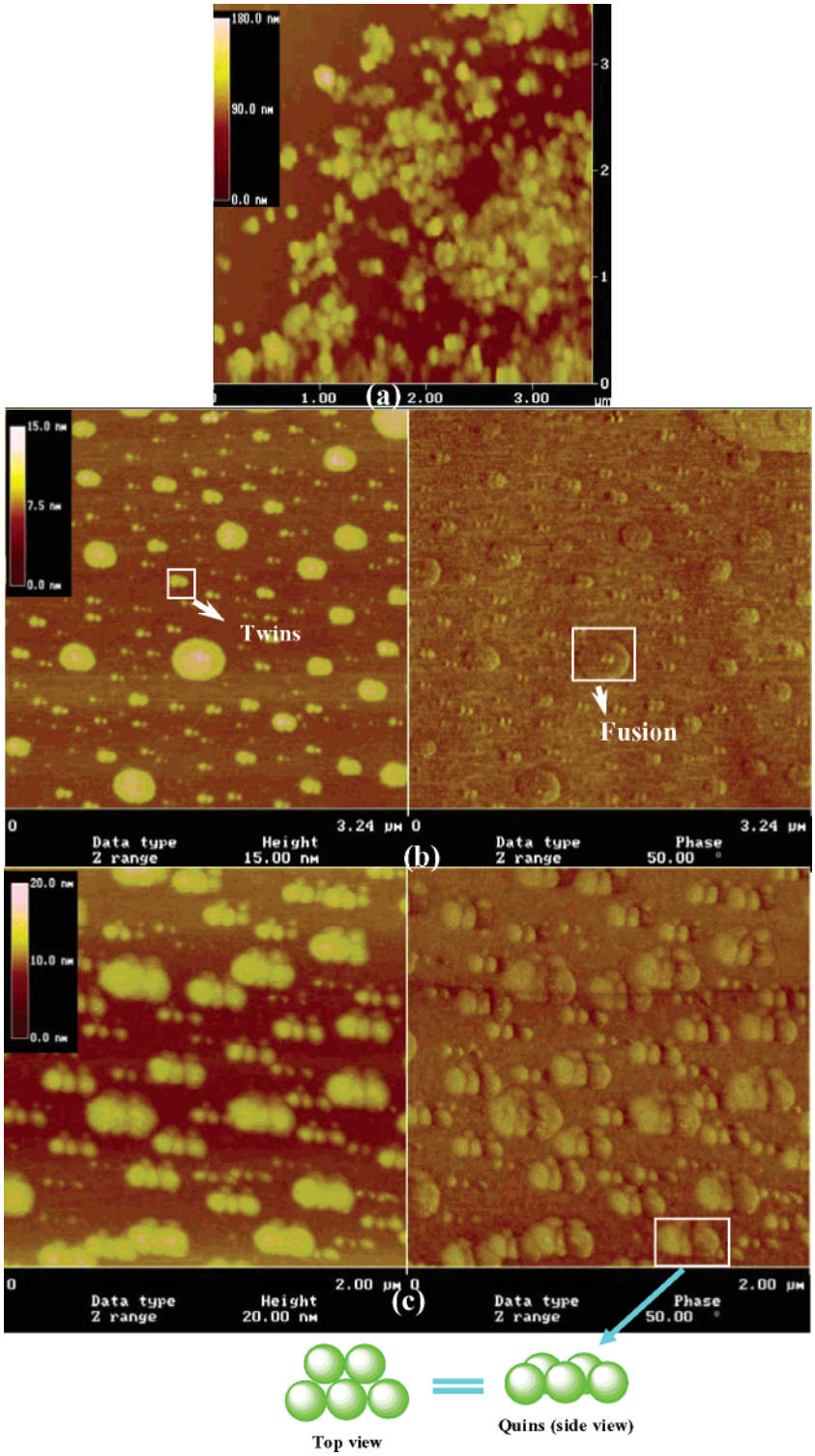

Figure 6. AFM images (topography and phase) of the PAMAM-Ph G0 (a), G1 (b) and G2 (c) aggregates deposited on the mica surface, displaying the multiple aggregate "twins" and "quins" consisting of two and five individual aggregates.

technique as reported by Chu, Zhou, and Wu[41] and fluorescence quenching technique as reported by Strauss and Thomas.[43] We attempted to utilize the above techniques to determine the aggregation numbers but have not been successful. The aggregation numbers determined by fluorescence techniques based on a probe/quencher combination are generally accepted for surfactant-like spherical micelles.[44] The basic principle of this technique is the Poisson statistical quenching when the probe and quencher molecules are partitioned into micellar micro-

(42) To obtain reliable data, the thickness of hydrophobic interphase was measured from TEM images without electron staining. The reason for this is it was found that the thickness observed from TEM images with negative staining is slightly larger than the actual thickness. This might be due to the negative uranyl acetate staining. In TEM images with negative staining, only the accessible area of the electron stainer was observed in black, which makes the relatively lighter area (apparent hydrophobic interphase) look slightly larger.

(43) (a) Chu, D.; Thomas, J. K. *Macromolecules* **1987**, *20*, 2133−2138. (b) Hsu, J.; Strauss, U. P. *J. Phys. Chem.* **1987**, *91*, 6238−6241. (c) Zdanowicz, V.; Strauss, U. P. *Macromolecules* **1993**, *26*, 4770−4773.

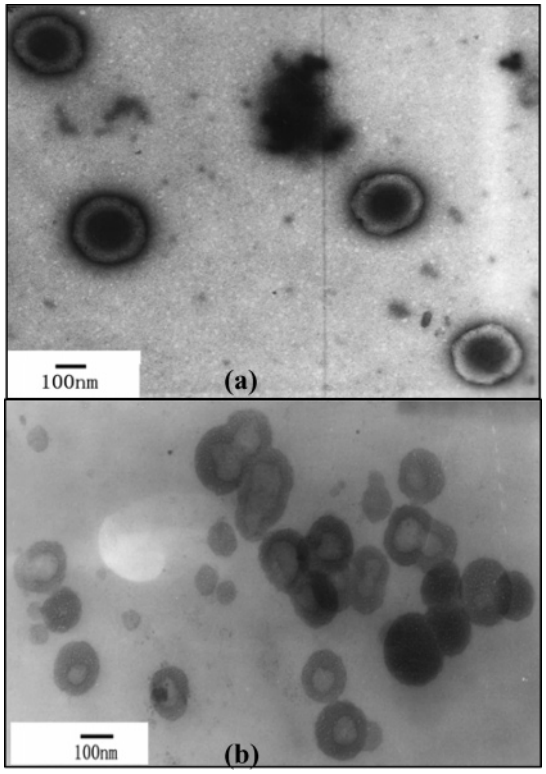

Figure 7. TEM images of the PAMAM-Ph G1 aggregates in water with negative staining (a) where the hydrophilic part was stained in black and without electron staining (b) that displays a reversed image. Concentration: 0.5 mg/mL.

domains. However, the exact measurement for some complex aggregates, such as cylindrical micells, microemulsions, vesicles, and bilayers, has been debated.[45] Although the laser light scattering technique can provide some useful information on aggregation behavior, it contains many hypotheses, which often leads to unreliable results.[41b]

In the present study, we used the geometric relation model proposed and developed by Tanford[46] and Israelachvili[47] to quantify the shape and size of aggregates. In brief, the geometric characteristics of an individual amphiphilic dendrimer should be strongly correlated to the shape and size of its aggregates. There are three critical geometric characteristics of the individual dendrimer as shown in Figure 10: (1) the optimal area occupied by the hydrophilic branches of dendrimers (a_0); (2) the volume of the individual dendrimer (v); and (3) the maximum extended length (l_d), which is comparable to the radius of the dendrimer molecule. Based on the dendrimer density 1.232 g/cm^3 as reported by Tomalia,[48] the volume of the individual dendrimer (v) can be determined from its molecular weight (M). The average sizes of the vesicles and the average thickness of the

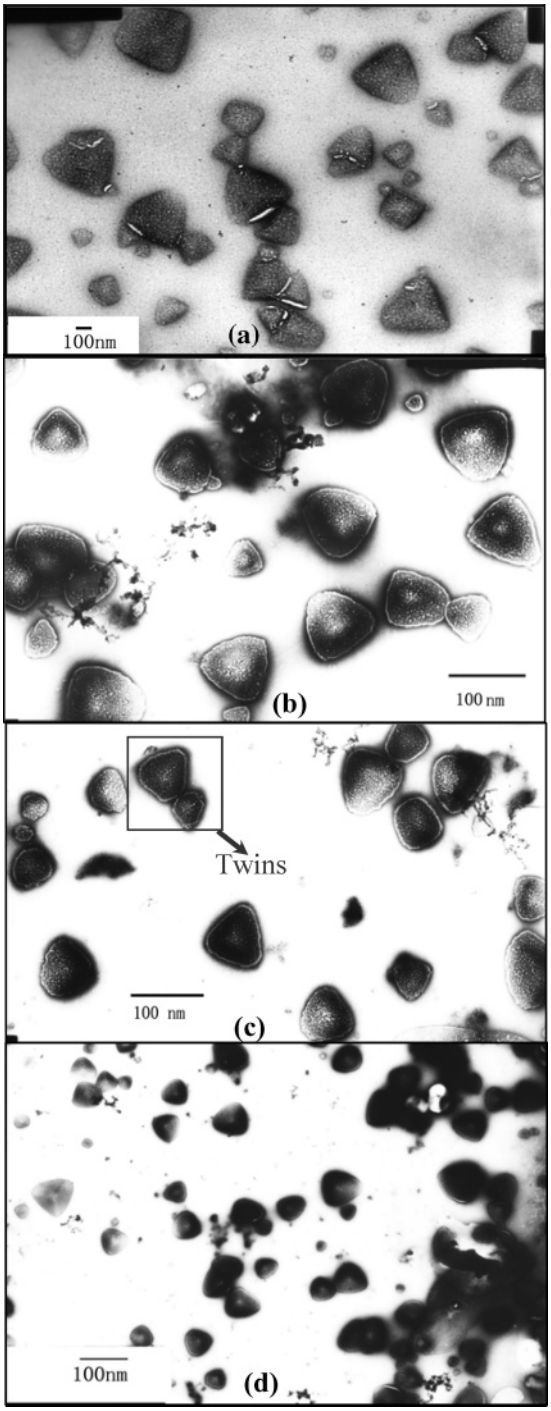

Figure 8. TEM images of triangle-like aggregates of PAMAM-Py G0 without electron staining (a) and PAMAM-Py G1 (b), G2 (c), and G3 (d) with negative staining in water. Concentration: 0.5 mg/mL.

hydrophobic interphase between bilayers were determined from 50 transmission images (about 900 aggregates). From the average size and thickness, the aggregation number of inner and outer layers can be determined by dividing the overall occupied volume by the volume of the individual dendrimer. The a_0 value is subsequently obtained from the overall spherical area divided by the aggregation number.

From the above data, the critical packing parameter (P_c) can be calculated using the equation: $P_c = v/a_0 l_c$.[47,39b] The P_c value is a key parameter to predicting the shape and size of aggregates[39] that will produce a minimum in free energy for a

(44) (a) Hansson, P.; Schneider, S.; Lindman, B. *J. Phys. Chem. B* **2002**, *106*, 9777−9793. (b) Bales, B. L.; Zana, R. *J. Phys. Chem. B* **2002**, *106*, 1926−1939. (c) Vasilescu, M.; Caragheorgheopol, A.; Caldararu, H. *Adv. Colloid Interface Sci.* **2001**, *89*, 169−194. (d) Hansson, P.; Jonsson, B.; Strom, C.; Soderman, O. *J. Phys. Chem. B* **2000**, *104*, 3496−3506. (e) Rodenhiser, A. P.; Kwak, J. C. T. *J. Phys. Chem. B* **1999**. *103*, 2970−2972.
(45) (a) Kramer, M. C.; Steger, J. R.; Hu, Y. X.; McCormick, C. L. *Macromolecules* **1996**, *29*, 1992−1997. (b) Hu, Y. X.; Armentrout, R. S.; McCormick, C. L. *Macromolecules* **1997**, *30*, 3538−3546.
(46) Tanford, C. *The Hydrophobic Effect. Formation of Micelles and Biological Membranes*, 2nd ed.; Wiley: New York, 1980.
(47) . Israelachvili, J. *Intermolecular and Surface Forces*, 2nd ed.; Academic Press: San Diego, CA, 1991.
(48) . Topp, A.; Bauer, B. J.; Tomalia, D. A.; Amis, E. J. *Macromolecules* **1999**, *32*, 7232−7237.

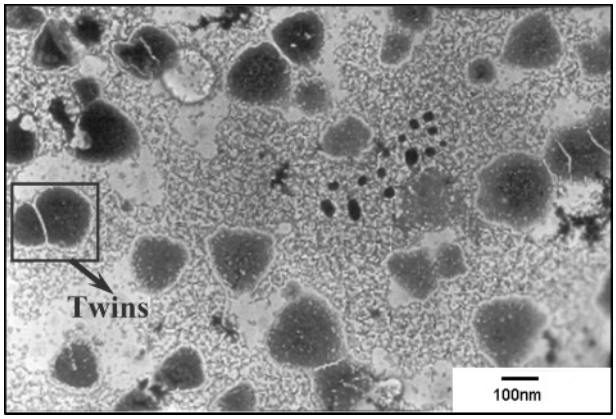

Figure 9. Representative TEM image of PAMAM-MNp G0 aggregates in water. Concentration: 0.5 mg/mL.

given amphiphilic dendritic structure. According to Israelachvili,[47] bilayer vesicular structures can be generated only if $0.5 \leq P_c \leq 1$. If $P_c < 0.33$, spherical micelles can be formed. If $0.33 \leq P_c \leq 0.5$, one can predict the formation of cylindrical or disk-shaped micelles. If $P_c > 1.0$, reversed or inverted micelles can be formed. These packing parameters provide the detailed aggregate characteristics of dendrimers as listed in Table 3. The P_c values for PAMAM-MNp G0−3 were found to be in the range of 0.5−1.0 and tend to decrease with increasing generation, suggesting that the aggregates possess bilayer vesicular structures. The theoretical prediction is in agreement with the actual observation from TEM. The same trend was observed for PAMAM-BNp aggregates.

For PAMAM-MNp aggregates, their average aggregation numbers ($\langle N \rangle$) decrease from 7.9×10^4 for G0 to 4.0×10^3 for G3, which is close to the aggregation number ($\sim 1.2 \times 10^4$) of bilayer vesicles made from C_{60} fullerene bearing hydrophilic groups reported by Zhou and Chu.[41a] The aggregation numbers of these dendrimer- and C_{60}-based vesicles are considerably larger than those of the vesicles derived from traditional ionic ($\langle N \rangle = 50-100$)[49a,b] and nonionic ($\langle N \rangle = 100-1000$)[49c,d] surfactants as well as diblock copolymers ($\langle N \rangle = 50-1000$).[49e−g] This is understandable because of their common features: instead of the flexible hydrophobic tails of traditional amphiphilic surfactants and diblock copolymers, both dendrimer- and C_{60}-based amphiphilic compounds possess rigid and bulky hydrophobic moieties with a dominant intrinsic geometric constraint. At the same generation, PAMAM-MNp aggregates show the larger aggregation numbers and P_c value than PAMAM-BNp aggregates. This is attributed to the relative size of hydrophobic and hydrophilic portions of individual dendrimer. The hydrophobic headgroups of PAMAM-BNp are bulky and more crowded as compared to that of PAMAM-MNp. For PAMAM-Py aggregates, these packing parameters are difficult to be assessed reliably because they are nonspherical.

Dendrimer Exchanges and Fluorescence Resonance Energy Transfer. As an in-depth study, we utilized the fluorescence resonance energy transfer (FRET) between pyrene and naphthalene chromophores to obtain further characterization on these dendrimer-based self-assemblies. FRET is known to depend on the following three factors:[32] (1) the extent of spectral overlap of acceptor absorption and donor emission, (2) the quantum yields of the donor, and (3) the distance between the donor and acceptor. FRET is a long-range and through-space interaction, which is independent of the intervening medium between donor and acceptor, such as solvents, chemical bonds, and polymer backbones.[50−52] The distance dependence of FRET has been employed as a "spectroscopic ruler" for a variety of applications, such as distance measurement between donor and acceptor,[51a,b] protein folding,[51c,d] conformational changes,[51e,f] macromolecular associations,[51g] membrane fusion, and lipid exchange.[51h] The photophysical phenomenon of FRET between donor and acceptor covalently attached to a polymer has been termed "photo harvesting" by Webber [52] and the "antenna effect" by Guillet.[53] The naphthalene/pyrene energy transfer pair has been employed to study the compatibility, thermo-reversible phase transition, and steric hindrance of polymers by Morawetz,[54a] Winnik,[54b] and Webber.[52b] In our previous work, we attempted to employ FRET to measure the bilayer thickness of vesicles made from amphiphilic copolymers. But, it is unsuccessful. The reason for this is that the bilayer thickness of vesicles from amphiphilic copolymer is generally in the range of 100−200 Å, which exceeds the effective range measured by FRET (20−90 Å).

In the present study, we have designed a control experiment in an effort to determine the bilayer thickness of dendrimer-based vesicles by changing the ratio of PAMAM-Py to PAMAM-MNp aggregates in the mixture for FRET measurement. Thus, 9.0 mL of PAMAM-Py aggregates (1.5×10^{-4} M) was mixed with 1.0 mL of PAMAM-MNp aggregates (1.5×10^{-4} M). At the excitation wavelength of 290 nm where the radiation is mostly absorbed by the naphthalene moiety, the fluorescence of the mixed aggregates was observed mostly from the pyrene chromophore with a relatively weak residual fluorescence of the naphthalene chromophore as shown in the inset (A and B) of Figure 12. This indicates that FRET occurs from the naphthalene to pyrene chromophore.

Figure 12 shows the time-resolved fluorescence spectra of the mixed aggregates of PAMAM-MNp G1 (1.5×10^{-4} M, 1.0 mL) and PAMAM-Py G1 (1.5×10^{-4} M, 9.0 mL). At the excitation wavelength of 295 nm and emission wavelength of 345 nm, the fluorescence decay was fitted by a single-

(49) (a) Benrraou, M.; Bales, B. L.; Zana, R. *J. Phys. Chem. B* **2003**, *107*, 13432−13440. (b) Srinivasan, V.; Blankschtein, D. *Langmuir* **2003**, *19*, 9932−9945. (c) Li, Y.; McMillan, C. A.; Bloor, D. M.; Penfold, J.; Warr, J.; Holzwarth, J. F.; Wyn-Jones, E. *Langmuir* **2000**, *16*, 7999−8004. (d) Kamenka, N.; Chevalier, Y.; Zana, R. *Langmuir* **1995**, *11*, 3351−3355. (e) Alexandridis, P.; Hatton, T. A. *Colloid Surf., A* **1995**, *96*, 1−46. (f) Yusa, S.; Sakakibara, A.; Yamamoto, T.; Morishima, Y. *Macromolecules* **2002**, *35*, 10182−10188. (g) Lysenko, E. A.; Bronich, T. K.; Slonkina, E. V.; Eisenberg, A.; Kabanov, V. A.; Kabanov, A. V. *Macromolecules* **2002**, *35*, 6344−6350.

(50) Calzaferri, G.; Huber, S.; Maas, H.; Minkowski, C. *Angew Chem., Int. Ed.* **2003**, *42*, 3732−3758.

(51) (a) Brogan, A. P.; Widger, W. R.; Kohn, H. *J. Org. Chem.* **2003**, *68*, 5575−5587. (b) Cha, A.; Snyder, G. E.; Selvin, P. R.; Bezanilla, F. *Nature* **1999**, *402*, 809−813. (c) Lipman, E. A.; Schuler, B.; Bakajin, O.; Eaton, W. A. *Science* **2003**, *301*, 1233−1235. (d) Schuler, B.; Lipman, E. A.; Eaton, W. A. *Nature* **2002**, *419*, 743−747. (e) Rice, S.; Lin, A. W.; Safer, D.; Hart, C. L.; Naber, N.; Carragher, B. O.; Cain, S. M.; Pechatnikova, E.; Wilson-Kubalek, E. M.; Whittaker, M.; Pate, E.; Cooke, R.; Taylor, E. W.; Milligan, R. A.; Vale, R. D. *Nature* **1999**, *402*, 778−784. (f) Remy, I.; Wilson, I. A.; Michnick, S. W. *Science* **1999**, *283*, 990−993. (g) Varma, R.; Mayor, S. *Nature* **1998**, *394*, 798−801.(h) Mochizuki, N.; Yamashita, S.; Kurokawa, K.; Ohba, Y.; Nagai, T.; Miyawaki, A.; Matsuda, M. *Nature* **2001**, *411*, 1065−1068.

(52) (a) Webber, S. E. *Chem. Rev.* **1990**, *90*, 1469−1482. (b) Fox, S. L.; Chan, J. C.; Kiserow, D. J.; Ramireddy, C.; Munk, P.; Webber, S. E. *Adv. Chem. Ser.* **1996**, *248*, 141−162.

(53) Guillet, J. E.; Rendall, W. A. *Macromolecules* **1986**, *19*, 224−230.

(54) (a) Morawetz, H. *J. Polym. Sci., Part A: Polym. Chem.* **1999**, *37*, 1725−1735. (b) Mizusaki, M.; Morishima, Y.; Winnik, F. M. *Macromolecules* **1999**, *32*, 4317−4326. (c) Zhao, C. L.; Wang, Y.; Hruska, Z.; Winnik, M. A. *Macromolecules* **1990**, *23*, 4082−4087. (d) Winnik, F. M. *Macromolecules* **1989**, *22*, 734−742, 55.

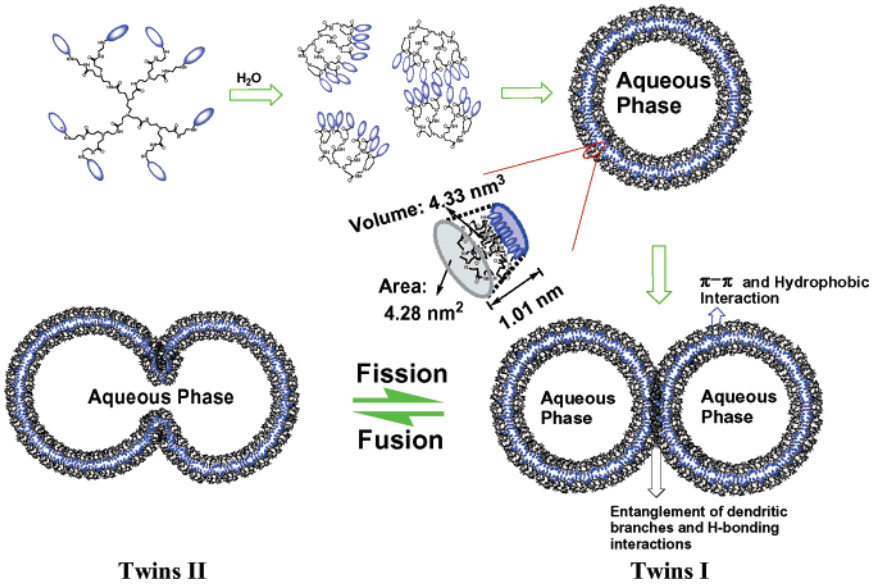

Figure 10. Schematic illustration of the vesicular formation and "twins I" and "twins II" structures for PAMAM-MNp G1. Two spherical vesicles were attached by the entanglement and H-bonding interaction of dendritic branches to form "twins I". Further fusion leads to the formation of the "twins II" structure. Hydrophobic aromatic chromophores are shown in blue, and the hydrophilic branches are in black.

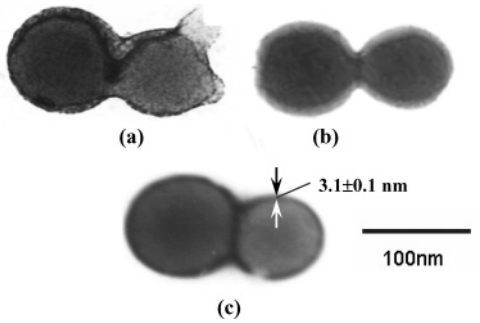

Figure 11. Representative TEM images of "twins II" structures for PAMAM-BNp G1 (a) and G2 (b) aggregates and TEM image without negative staining of "twins I" structure for the mixed aggregates of PAMAM-MNp G1 (1.5×10^{-4} M, 1.0 mL) and PAMAM-Py G1 (1.5×10^{-4} M, 9.0 mL) (c) displaying the thickness of hydrophobic interphase (3.1 ± 0.1 nm).[42]

Table 2. Critical Aggregation Concentration (CAC) of PAMAM-Py G0−3 and PAMAM-MNp G0−3 in Water

PAMAM-Py				
	G0	G1	G2	G3
CAC/M	9.70×10^{-6}	3.67×10^{-6}	2.10×10^{-7}	1.52×10^{-7}
PAMAM-MNp				
	G0	G1	G2	G3
CAC/M	1.70×10^{-5} (7.43×10^{-6})[a]	1.25×10^{-5}	0.98×10^{-5}	1.24×10^{-6} (7.41×10^{-7})[a]

[a] CAC value for PAMAM-BNp aggregates.

Table 3. Spherical Aggregate Characteristics of PAMAM-MNp G0−3 and PAMAM-BNp G0−3 in Water

PAMAM-MNp				
	G0	G1	G2	G3
M/g mol^{-1}	1409	3214	6807	14 044
$\langle R \rangle_{outer}$[a]/nm	90.3	82.7	58.6	40.8
υ/nm^3 [b] (per dendrimer)	1.90	4.33	9.18	18.9
l_d/nm[c] (per dendrimer)	0.768	1.01	1.30	1.65
$\langle l_h \rangle$[d]/nm	2.3	3.0	3.4	2.7
$\langle N \rangle_{outer}$[e]	4.1×10^4	2.0×10^4	5.9×10^3	2.2×10^3
$\langle N \rangle_{inner}$	3.8×10^4	1.8×10^4	5.0×10^3	1.8×10^3
a_0/nm^2 [f] (per dendrimer)	2.5	4.3	7.1	12
P_c[g]	0.989	0.997	0.995	0.955
PAMAM-BNp				
	G0	G1	G2	G3
M/g mol^{-1}	2303	5000	10379	21188
$\langle R \rangle_{outer}$[a]/nm	68.9	57.5	48.3	40.6
υ/nm^3 [b] (per dendrimer)	3.10	6.74	14.0	28.6
l_d/nm[c] (per dendrimer)	0.905	1.17	1.50	1.90
$\langle l_h \rangle$[d]/nm	2.5	3.2	3.3	3.2
$\langle N \rangle_{outer}$[e]	1.7×10^4	7.1×10^3	3.0×10^3	1.3×10^3
$\langle N \rangle_{inner}$	1.5×10^4	6.0×10^3	2.5×10^3	0.9×10^3
a_0/nm^2 [f] (per dendrimer)	3.5	5.8	9.4	16
P_c[g]	0.979	0.993	0.993	0.941

[a] Average radius $\langle R \rangle$ of aggregates directly observed from AFM and TEM. [b] Volume of the individual dendrimer (υ). [c] Maxmum extended length (l_d) of dendrimers, which is comparable to the radius of dendrimer molecule. [d] Average thickness $\langle l_h \rangle$ of hydrophobic interphase between bilayer directly observed from TEM. [e] Average aggregation numbers of outer and inner monolayer ($\langle N \rangle_{outer}$ and $\langle N \rangle_{inner}$). [f] Optimal area occupied by the hydrophilic branches of dendrimers (a_0). [g] Critical packing parameter ($P_c = \upsilon/a_0 l_d$).

exponential curve. The fitted lifetime is 8.87 ns assigned to the emission lifetime of naphthalene chromophore. With increasing emission wavelength, the decay curve becomes broader. The fluorescence decay was fitted by a dual exponential curve. An increasing amount of relative long lifetime (31.4 ns) emission was observed, which is assigned to the emission lifetime of pyrene chromophores. The time-resolved spectra confirm that the nonradiative energy transfer occurs from the naphthalene to pyrene chromophore in the mixed aggregates, suggesting that there is an exchange of dendrimer molecules between aggregates. Therefore, these aggregates are not isolated from each other.

It is well-known that the diffusion of the individual molecule of the outer monolayer is much easier than that of the inner monolayer as described by Marrink and Mark[39a] and that the individual molecules located in the outer layer almost do not exchange with ones in the inner layer of vesicles.[39b] Therefore, the exchanges of individual dendrimer due to its diffusion mostly occurred in the outer monolayer of vesicular aggregates. For

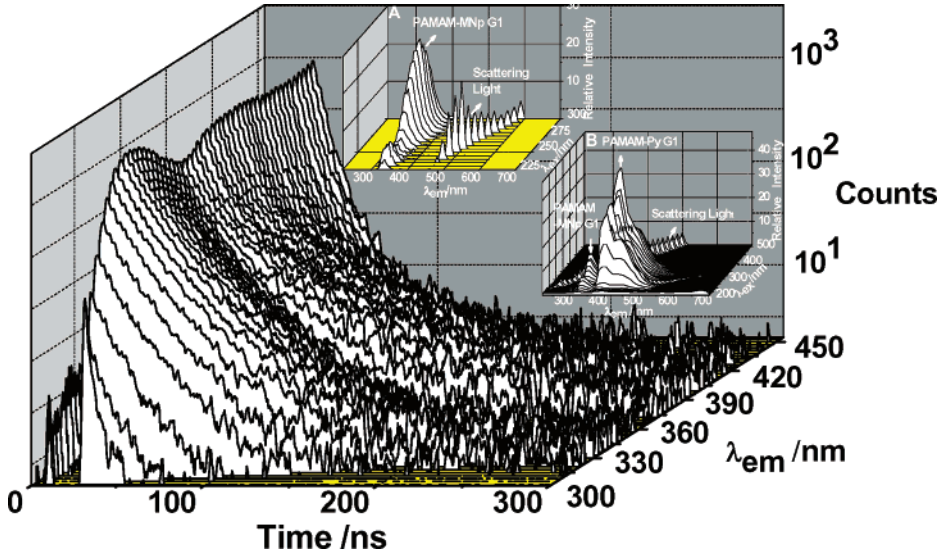

Figure 12. Time-resolved fluorescence decay of the mixed aggregates of PAMAM-MNp G1 (1.5×10^{-4} M) and PAMAM-Py G1 (1.5×10^{-4} M) in a 1:9 volume ratio in H_2O. The excitation wavelength was 290.0 nm, and the emission wavelength was varied from 300.0 to 460.0 nm in 3.0 nm steps. Inset: Steady-state three-dimensional fluorescence (emission-excitation-intensity) spectra of PAMAM-MNp G1 aggregate (1.5×10^{-4} M) before (A) and after (B) mixing PAMAM-Py G1 aggregates (1.5×10^{-4} M) in a 1:9 volume ratio.

the mixed aggregates of PAMAM-MNp (1.5×10^{-4} M)/PAMAM-Py (1.5×10^{-4}) in a 1:9 volume ratio, such exchanges should result in about 10% of mixed bilayer vesicles, where the inner monolayer mostly consists of naphthalene chromophores, while the outer monolayer mostly consists of pyrene chromophores as illustrated in Figure 13. When a naphthalene chromophore is excited at 290 nm, the fluorescence emission from pyrene was indeed observed at 378−400 nm due to FRET. Other aggregates (about 90%) mostly consist of pyrene chromophores with a few naphthalene chromophores. They almost do not absorb and are not excited at 290 nm. FRET from pyrene to naphthalene is negligible.

The FRET from naphthyl chromophores of the inner layer to the pyrenyl chromophores of the outer layer can be thus employed as a spectroscopic ruler[49] to measure the hydrophobic interphase thickness of the mixed vesicles. When the efficiency of FRET is 50%, the distance between acceptor and donor is called the Förster distance.[32] On the bases of the absorption and emission spectra of model compounds MNp and MPy, Förster distance (R_0) was calculated by using the following equation:[32]

$$R_0^{\,6} = [9000(\ln 10)k^2Q_D]/128\pi^5Nn^4\,[\int_0^\infty F_D(\lambda)\,\epsilon_A(\lambda)\,\lambda^4\,d\lambda]/[\int_0^\infty F_D(\lambda)\,d\lambda] = 0.211^6[k^2n^{-4}Q_D\,J(\lambda)] \quad (2)$$

where Q_D is the fluorescence quantum yields of the energy donor naphthalene, n is the refractive index of the solvent, $J(\lambda)$ is the spectral overlap integral, ϵ_A is the molar extinction coefficient of the acceptor pyrene, and $F_D(\lambda)$ is the fluorescence spectrum of the donor naphthalene on a wavelength (λ) scale. The R_0 value forthe MNp−MPy pair was calculated to be 26.0 Å, which is in the range 20−60 Å for a typical donor−acceptor pair. This value is close to 26.6 Å reported by McCormick[45] and Winnik[54c,d] and Ringsdorf[55] for a naphthalene/pyrene pair. For the dendrimers, the spectral overlap integral $J(\lambda)$ was calculated to be 3.521×10^{14} M^{-1} $cm^{-1}(nm)^4$ from the absorption spectrum of PAMAM-MNp G0 aggregates and the emission spectrum of PAMAM-Py G0 aggregates, after correction for the nonradiative self-quenching of adjacent naphthyl or pyrenyl chromophores within the same monolayer. The spectral overlap integral calculated for other dendrimer generations is essentially the same. The R_0 value was subsequently calculated to be 20.8 ± 0.2 Å. The transfer efficiency (E) was determined by calculating the quantum yields of naphthyl chromophores of PAMAM-MNp aggregates before (Q_D) and after (Q_{AD}) mixing with PAMAM-Py aggregates according to the following equation.[32]

$$E = 1 - Q_{AD}/Q_D \quad (3)$$

For the mixed aggregates of PAMAM-MNp G0 (1.5×10^{-4} M) and PAMAM-Py G0 (1.5×10^{-4} M) in a 1: 9 volume ratio, the E value is calculated to be 0.46. For PAMAM-MNp G1/PAMAM-Py G1 under the same mixing condition, the E value is calculated to be 0.11. For PAMAM-MNp G2/PAMAM-Py G2, the E value is 0.07. For PAMAM-MNp G3/PAMAM-Py G3, the E value is 0.21. Based on the R_0 and E values, the average distance (r) between naphthyl and pyrenyl chromophores was determined by using the following equation:

$$E = R_0^{\,6}/(R_0^{\,6} + r^6) \quad (4)$$

The average thickness of hydrophobic interphase between bilayer is equal to the average distance (r), which was calculated to be 2.04 nm for the PAMAM-MNp G0/PAMAM-Py G0 mixed aggregates, 2.95 nm for PAMAM-MNp G1/PAMAM-Py G1, 3.20 nm for PAMAM-MNp G2/PAMAM-Py G2, and 2.59 nm for PAMAM-MNp G3/PAMAM-Py G3, respectively as shown in Figure 13.

To further confirm the fluorescence results, the mixed aggregates were examined with TEM to measure the interphase thickness directly. As shown in Figure 11c, the average thickness of hydrophobic interphase measured from TEM is 3.1 ± 0.1 nm,[42] which is in excellent agreement with 2.95 nm from FRET.

(55) Ringsdorf, H.; Sackmann, E.; Simon, J.; Winnik, F. M. *Biochim. Biophys. Acta* **1993**, *1153*, 335−344.

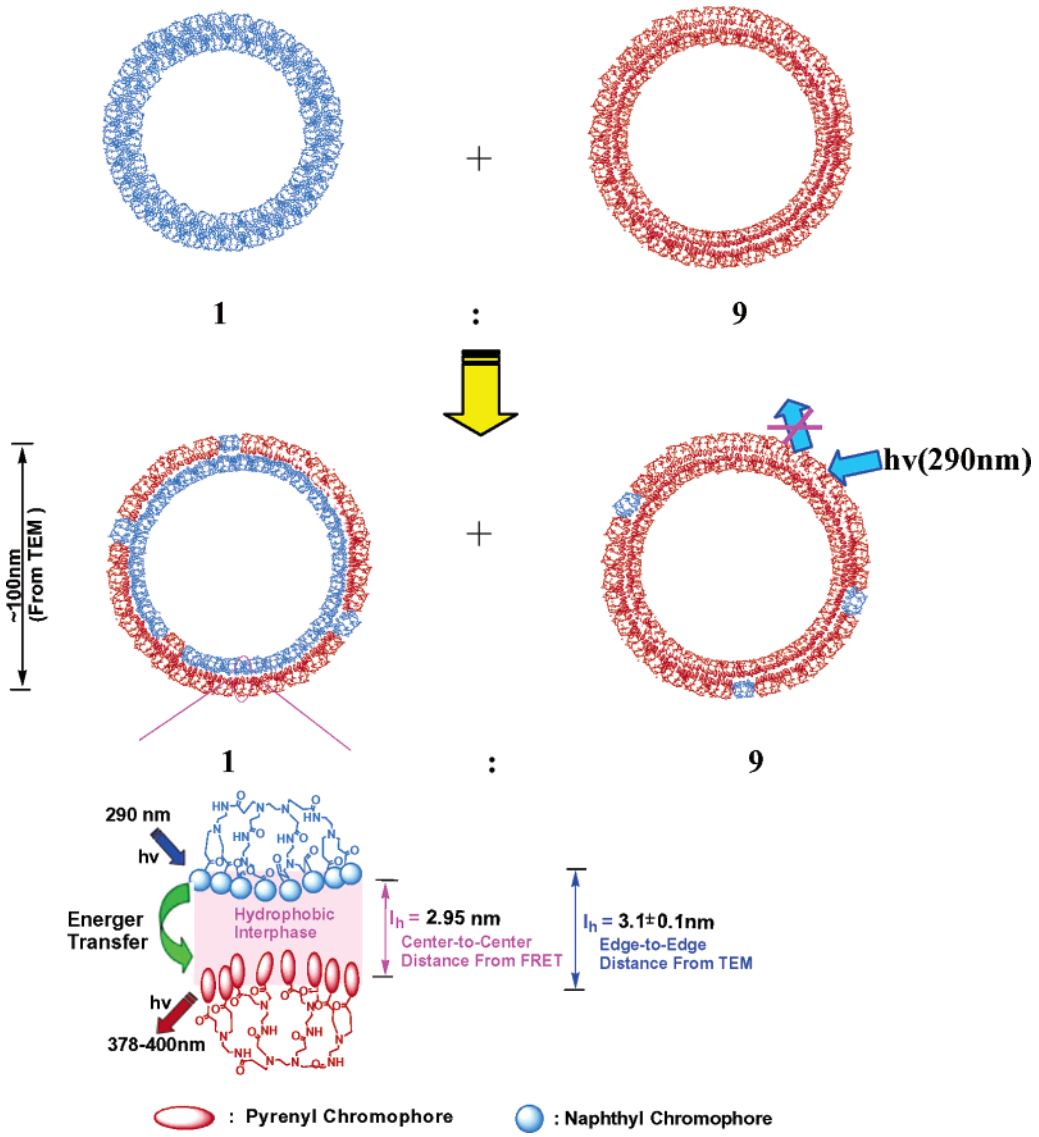

Figure 13. Schematic illustration of dendrimer exchanges for the mixed aggregates of PAMAM-MNp G1 (1.5×10^{-4} M) and PAMAM-Py G1 (1.5×10^{-4} M) in water in a 1:9 volume ratio. In the mixed bilayer structures (~10%), the outer monolayer mostly consists of pyrenyl chromophores shown in red, and the inner monolayer mostly consists of naphthyl chromophores shown in blue. Fluorescence resonance energy transfer (FRET) occurs from the inner to the outer monolayer upon photoexcitation at 290 nm. Other aggregates (~90%) mostly consist of pyrenyl chromophores, where there is almost no emission observed at the excitation wavelength 290 nm.

The slightly lower value might be due to the fact the thickness measured from FRET is a center-to-center distance of aromatic chromophores of hydrophobic interphase, while the thickness observed from TEM is an edge-to-edge distance as illustrated in Figure 13.

Conclusions

PAMAM Dendrimers G0−5 were peripherally modified with naphthyl, pyrenyl, and dansyl chromophores. Their fluorescence behavior was found to depend strongly on the dendritic architecture and correlate with the transition of dendritic architecture from an extended structure at the lower generations to a three-dimensional globular shape at the higher generations (e.g., G4 or higher). AFM and TEM images show that these amphiphilic dendrimers at the low generations (G0−3) can self-organize into bilayer vesicles in water. The self-organization is likely induced by the $\pi-\pi$ interaction of the peripheral aromatic chromophores, the H-bonding interaction of interior amidoamine units, and further entanglement of dendrimer branches. For these dendrimers with peripheral pyrenyl chromophores, irregular triangle-like vesicles were observed in water. In contrast to the vesicles from traditional surfactants and amphiphilic block copolymers, the dendrimer-based vesicles have several distinct features: (1) The vesicles possess a thin wall (e.g., hydrophobic interphase of ca. 2.3−3.4 nm) as compared to that from amphiphilic block copolymers (10−20 nm). (2) The vesicles are very adhesive due to the dendrimer branches located in the outer layer. A large number of interesting "twins" and "quins" vesicular aggregates consisting of two and five vesicles, respectively, were observed for the first time. The average diameter and aggregation number of the vesicles were found to decrease with increasing generation. The critical aggregation concentration value shows that the vesicle formation is favored in the order of G3 > G2 > G1 > G0. However, higher generations, i.e., G4 and G5, do not form ordered aggregates. Based on the fluorescence resonance energy transfer between

naphthyl and pyrenyl chromophores in a mixed vesicle system, an intervesicular exchange of dendrimer molecules was revealed, and the hydrophobic interphase thickness of the mixed vesicles was determined to be 2.04−3.20 nm, which agrees well with the thickness observed with TEM.

Acknowledgment. We are most grateful to the National Natural Science Foundation of China (NSFC Grant No. 20340420002 and No. 20374002) for the financial support. Partial support from the Nanotechnology Institute of Southeastern Pennsylvania is also acknowledged.

Supporting Information Available: Materials, measurements, spectral characterization of model compounds MNp, BNp, MPy, BPy and peripherally modified PAMAM dendrimers, i.e., PAMAM-Ph G2−5, PAMAM-DNS G0, G2−5, PAMAM-Py G0, 2−5, PAMAM-MNp G0−5, PAMAM-BNp G0−5; Stern−Volmer plots for the fluorescence quenching of PAMAM-BNp by triethylamine, PAMAM-MNp by triethylamine, and PAMAM-Py by *N*,*N*-dimethylphenylamine; critical aggregation concentration of PAMAM-Py G3, PAMAM-BNp G3, and PAMAM-MNp G3 determined by fluorescence methods; reaction dynamic curves of the peripheral modification of PAMAM G2 and G3; fluorescence spectra of PAMAM-MNp G2−4 with different reaction extents; AFM images of the PAMAM-Py G4−5 and PAMAM-BNp G5 aggregates deposited on the mica surface. This material is available free of charge via the Internet at http://pubs.acs.org.

JA048219R